A comprehensive study of hygroscopic properties of calcium- and magnesium-containing salts: implication for hygroscopicity of mineral dust and sea salt aerosols

Liya Guo,[1,5,a] Wenjun Gu,[1,5,a] Chao Peng,[2,5] Weigang Wang,[2] Yong Jie Li,[3] Taomou Zong,[4] Yujing Tang,[1] Zhijun Wu,[4] Qinhao Lin,[1] Maofa Ge,[2,5,6] Guohua Zhang,[1] Min Hu,[4] Xinhui Bi,[1] Xinming Wang,[1,5,6] Mingjin Tang[1,5,*]

1 State Key Laboratory of Organic Geochemistry and Guangdong Key Laboratory of Environmental Protection and Resources Utilization, Guangzhou Institute of Geochemistry, Chinese Academy of Sciences, Guangzhou 510640, China

2 State Key Laboratory for Structural Chemistry of Unstable and Stable Species, Institute of Chemistry, Chinese Academy of Sciences, Beijing, China

3 Department of Civil and Environmental Engineering, Faculty of Science and Technology, University of Macau, Avenida da Universidade, Taipa, Macau, China

4 State Key Joint Laboratory of Environmental Simulation and Pollution Control, College of Environmental Sciences and Engineering, Peking University, Beijing 100871, China

5 University of Chinese Academy of Sciences, Beijing 100049, China

6 Center for Excellence in Regional Atmospheric Environment, Institute of Urban Environment, Chinese Academy of Sciences, Xiamen 361021, China

[a] These two authors contributed equivalently to this work.

* Correspondence: Mingjin Tang (mingjintang@gig.ac.cn)

Abstract

Calcium- and magnesium-containing salts are important components for mineral dust and sea salt aerosols, but their physicochemical properties are not well understood yet. In this study, the hygroscopic properties of eight Ca- and Mg-containing salts, including $Ca(NO_3)_2 \cdot 4H_2O$, $Mg(NO_3)_2 \cdot 6H_2O$, $MgCl_2 \cdot 6H_2O$, $CaCl_2 \cdot 6H_2O$, $Ca(HCOO)_2$, $Mg(HCOO)_2 \cdot 2H_2O$, $Ca(CH_3COO)_2 \cdot H_2O$ and $Mg(CH_3COO)_2 \cdot 4H_2O$, were investigated using two complementary techniques. A vapor sorption analyzer was used to measure the change of sample mass with relative humidity (RH) under isotherm conditions, and the deliquescence relative humidities (DRH) for temperature in the range of 5-30 ^oC as well as water-to-solute ratios as a function of RH at 5 and 25 ^oC were reported for these eight compounds. DRH values showed large variation for these compounds; for example, at 25 ^oC DRH were measured to be ~28.5% for $CaCl_2 \cdot 6H_2O$ and >95% for $Ca(HCOO)_2$ and $Mg(HCOO)_2 \cdot 2H_2O$. We further found that the dependence of DRH on temperature can be approximated by the Clausius-Clapeyron equation. In addition, a humidity-tandem differential mobility analyzer was used to measure the change in mobility diameter with RH (up to 90%) at room temperature, in order to determine the hygroscopic growth factors of aerosol particles generated by atomizing water solutions of these eight compounds. All the aerosol particles studied in this work, very likely to be amorphous under dry conditions, started to grow at very low RH (as low as 10%) and showed continuous growth with RH. The hygroscopic growth factors at 90% RH were found to range from 1.26±0.04 for $Ca(HCOO)_2$ to 1.79±0.03 for $Ca(NO_3)_2$, and the single hygroscopicity parameter ranged from 0.09-0.13 for $Ca(CH_3COO)_2$ to 0.49-0.56 for $Ca(NO_3)_2$. Overall, our work provides a comprehensive investigation of the hygroscopic properties of these Ca- and Mg-containing salts, largely improving our knowledge in the physicochemical properties of mineral dust and sea salt aerosols.

1 Introduction

Mineral dust, mainly emitted from arid and semi-arid regions with an annual flux of ~2000 Tg, is one of the most abundant types of aerosols in the troposphere (Textor et al., 2006; Ginoux et al., 2012). Mineral dust aerosol affects the climate system directly by scattering and absorbing solar and terrestrial radiation (Formenti et al., 2011; Ridley et al., 2016; Chen et al., 2017) and indirectly by serving as cloud condensation nuclei (CCN) and ice nucleating particles (INPs) (Hoose and Moehler, 2012; Creamean et al., 2013; Cziczo et al., 2013; Tang et al., 2016a). In addition, deposition of mineral dust particles is an important source of several nutrient elements (Fe and P, for example) for many ecosystems around the globe, thus having significant impacts on biogeochemical cycles in these regions (Jickells et al., 2005; Mahowald et al., 2009; Mahowald et al., 2011; Zhang et al., 2015).

Mineral dust aerosol has an average lifetime of 2-7 days in the atmosphere and can thus be transported over thousands of kilometers (Textor et al., 2006; Uno et al., 2009). During transport mineral dust particles may undergo heterogeneous reactions with trace gases, impacting the abundance of a number of important reactive trace gases both directly and indirectly (Usher et al., 2003; Crowley et al., 2010; Romanias et al., 2012; Tang et al., 2017). These reactions can also lead to change in chemical composition of mineral dust particles (Usher et al., 2003; Li and Shao, 2009; Li et al., 2010; Tang et al., 2012; Romanias et al., 2016) and thereby modification of their physicochemical and optical properties (Krueger et al., 2003; Vlasenko et al., 2006; Liu et al., 2008b; Sullivan et al., 2009; Tang et al., 2016a; Pan et al., 2017). Mineral dust particles contain substantial amounts of carbonates, including $CaCO_3$ (calcite) and $CaMg(CO_3)_2$ (dolomite) (Nickovic et al., 2012; Formenti et al., 2014; Jeong and Achterberg, 2014; Journet et al., 2014; Scanza et al., 2015). These carbonates are largely insoluble and have very low hygroscopicity

(Sullivan et al., 2009; Tang et al., 2016a); however, their reactions with acidic gases in the troposphere can form Ca- and Mg-containing salts with higher hygroscopicity (Gibson et al., 2006; Liu et al., 2008b; Sullivan et al., 2009; Tang et al., 2016a), such as $Ca(NO_3)_2$ and $Mg(NO_3)_2$. For example, numerous laboratory and field studies have found that due to the formation of $Ca(NO_3)_2$ and $CaCl_2$ from heterogeneous reactions with nitrogen oxides (Goodman et al., 2000; Liu et al., 2008a; Li et al., 2010; Tang et al., 2012; Tan et al., 2016) and HCl (Santschi and Rossi, 2006), solid $CaCO_3$ particles could be converted to aqueous droplets under tropospheric conditions (Krueger et al., 2003; Laskin et al., 2005; Liu et al., 2008b; Shi et al., 2008; Tobo et al., 2010). In addition, $MgCl_2$ and $CaCl_2$ are important components in sea salt aerosol (as known as sea spray aerosol). The presence of $MgCl_2$ and $CaCl_2$, in addition to NaCl, can alter the hygroscopicity of sea salt aerosol (Gupta et al., 2015; Zieger et al., 2017); to be more specific, the hygroscopicity of sea salt was found to be significantly smaller than pure NaCl. Furthermore, the CCN activity of saline mineral dust was explored (Gaston et al., 2017), and good correlations were found between the CCN activities of saline mineral dust particles and the abundance of the soluble components (e.g., $CaCl_2$) they contained.

Nevertheless, hygroscopic properties of $Ca(NO_3)_2$, $Mg(NO_3)_2$, $CaCl_2$ and $MgCl_2$ have not been completely understood, especially in the two following aspects. First, hygroscopic growth factors were only measured by one or two previous studies for $Ca(NO_3)_2$ (Gibson et al., 2006; Jing et al., 2018), $Mg(NO_3)_2$ (Gibson et al., 2006), $CaCl_2$ (Park et al., 2009) and $MgCl_2$ aerosols (Park et al., 2009). Considering the importance of these compounds in the troposphere, additional measurements of their hygroscopic growth are clearly warranted. In addition, tropospheric temperatures range from ~200 to ~300 K; however, the effects of temperature on their phase

transitions and hygroscopic growth remain largely unclear (Kelly and Wexler, 2005), due to lack of experimental data below room temperature.

Small carboxylic acids, such as formic and acetic acids, are abundant in the troposphere (Khare et al., 1999), and previous studies suggested that heterogeneous reactions of mineral dust with formic and acetic acids are efficient (Hatch et al., 2007; Prince et al., 2008; Tong et al., 2010; Ma et al., 2012; Tang et al., 2016b). It was shown that calcium and magnesium acetates were formed in heterogeneous reactions of gaseous acetic acid with MgO and $CaCO_3$ particles, leading to significant increase in particle hygroscopicity (Ma et al., 2012). However, only a few previous studies explored hygroscopic growth of $Mg(CH_3COO)_2$ and $Ca(CH_3COO)_2$, using techniques based on bulk samples (Wang et al., 2005; Ma et al., 2012; Pang et al., 2015). To our knowledge, hygroscopic growth factors have never been reported for $Ca(HCOO)_2$, $Mg(HCOO)_2$, $Ca(CH_3COO)_2$ and $Mg(CH_3COO)_2$ aerosol particles.

To better understand the hygroscopic properties of these Ca- and Mg-containing salts, two complementary techniques were employed in this work to investigate their phase transitions and hygroscopic growth. A vapor sorption analyzer, which measured the sample mass as a function of RH, was used to determine the DRH and solute-to-water ratios for $Ca(NO_3)_2{\cdot}4H_2O$, $Mg(NO_3)_2{\cdot}6H_2O$, $CaCl_2{\cdot}6H_2O$, $MgCl_2{\cdot}6H_2O$, $Ca(HCOO)_2$, $Mg(HCOO)_2{\cdot}2H_2O$, $Ca(CH_3COO)_2{\cdot}H_2O$ and $Mg(CH_3COO)_2{\cdot}4H_2O$ at different temperatures (5-30 ^oC). Furthermore, hygroscopic growth factors of $Ca(NO_3)_2$, $Mg(NO_3)_2$, $CaCl_2$, $MgCl_2$, $Ca(HCOO)_2$, $Mg(HCOO)_2$, $Ca(CH_3COO)_2$ and $Mg(CH_3COO)_2$ aerosol particles were determined at room temperature up to 90% RH, using a humidity-tandem differential mobility analyzer. This work would significantly increase our knowledge in the hygroscopicity of these compounds, hence leading to a better understanding of the physicochemical properties of mineral dust and sea salt aerosols.

2 Experimental section

Hygroscopic growth of Ca- and Mg-containing salts were investigated using two complementary techniques, i.e. a humidity-tandem differential mobility analyzer (H-TDMA) and a vapor sorption analyzer (VSA). Eight salts, all supplied by Aldrich, were investigated in this work, including $Ca(NO_3)_2 \cdot 4H_2O$ (>99%), $Mg(NO_3)_2 \cdot 6H_2O$ (99%), $CaCl_2 \cdot 6H_2O$ (>99%), $MgCl_2 \cdot 6H_2O$ (>99%), $Ca(HCOO)_2$ (>99%), $Mg(HCOO)_2 \cdot 2H_2O$ (98%), $Ca(CH_3COO)_2 \cdot H_2O$ (>99%) and $Mg(CH_3COO)_2 \cdot 4H_2O$ (99%).

2.1 H-TDMA experiments

H-TDMA measurements were carried out at Institute of Chemistry, Chinese Academy of Sciences, and the experimental setup was detailed in previous work (Lei et al., 2014; Peng et al., 2016). Hygroscopic growth of size-selected aerosol particles was determined by measuring their mobility diameters at different RH. An atomizer (MSP 1500) was used to generate aerosol particles. Solutions used for atomization were prepared using ultrapure water, and their typical concentrations were 0.3-0.4 g L^{-1}. After exiting the atomizer, an aerosol flow (300 mL/min) was passed through a Nafion dryer and then a diffusion dryer filled with silica gel to reach a final RH of <5%. The aerosol flow was then delivered through a neutralizer and the first differential mobility analyzer (DMA) to produce quasi-monodisperse aerosol particles with a mobility diameter of 100 nm. After that, the aerosol flow was transferred through a humidification section with a residence time of ~27 s to be humidified to a given RH. The humidification section was made of two Nafion humidifiers (MD-700-12F-1, Perma Pure) connected in series. The RH of the resulting aerosol flow was monitored using a dew-point meter, which had an absolute uncertainty of ±0.8% in RH measurement as stated by the manufacturer (Michell, UK). After humidification, the size distribution of aerosol particles was measured using a scanning mobility particle sizer

(SMPS) which consisted of the second DMA coupled with a condensation particle counter (TSI 3776). For the second DMA, the aerosol flow and the sheath flow were always maintained at the same RH. The flow rate ratios of the aerosol flow to the sheath flow were set to 1:10 for both DMA.

In our work, the hygroscopic growth factor (GF) is defined as the ratio of measured mobility diameters at a given RH to that at dry conditions:

$$GF = \frac{d}{d_0} \qquad (1)$$

where d_0 and d are the measured mobility diameters at <5% RH and at a given RH, respectively. In our work the dry mobility diameter selected using the first DMA was always 100 nm, and no shape factors were used to correct the dry particle diameters. Size distributions of all the eight types of aerosol particles, measured using the SMPS, were found to be unimode, as illustrated by Figure S1 (in the supplementary information) in which size distributions of $Ca(NO_3)_2$ aerosols at 4, 50 and 90% RH are displayed as an example. The TDMAinv algorithm (Gysel et al., 2009) was applied to the H-TDMA data.

All the experiments were carried out at room temperature (298±1 K), and in each experiment hygroscopic growth of aerosol particles was determined at 12 different RH, i.e. <5, 10, 20, 30, 40, 50, 60, 70, 75, 80, 85, and 90%. The absolute uncertainties in RH were estimated to be within ±2%. Hygroscopic growth of each compound was measured three times. The performance of the H-TDMA setup was routinely checked by measuring the hygroscopic growth of 100 nm $(NH_4)_2SO_4$ and NaCl aerosol particles. Good agreement between measured hygroscopic growth curves with those predicted using the E-AIM model (Clegg et al., 1998) was always found for $(NH_4)_2SO_4$ and NaCl aerosols, as detailed in our previous work (Jing et al., 2016; Peng et al., 2016).

2.2 VSA experiments

The vapor sorption analyzer (Q5000SA), which measured the mass of a bulk sample as a function of RH under isotherm conditions, was manufactured by TA Instruments (New Castle, DE, USA). These experiments were performed at Guangzhou Institute of Geochemistry, Chinese Academy of Sciences, and the instrument and experimental method were described elsewhere (Gu et al., 2017a; Gu et al., 2017b; Jia et al., 2018). Experiments could be conducted in a temperature range of 5-85 ^{o}C with an accuracy of ±0.1 ^{o}C and a RH range of 0-98% with an absolute accuracy of ±1%. The mass measurement had a range of 0-100 mg, and its sensitivity was stated to be <0.1 μg. Initial mass of samples used in an experiment was usually in the range of 0.5-1 mg.

Two different types of experiments were carried out. The mass hygroscopic growth was studied in the first type of experiments: after the sample was dried at <1% RH as a given temperature, RH was increased to 90% stepwise with an increment of 10% per step; after that, RH was set to 0% (the actual RH was measured to be <1%) to dry the sample again. The second type of experiments were conducted to measure DRH values: the sample was first dried at a given temperature, and RH was increased to a value which was at least 5% lower than the expected DRH; RH was then increased stepwise with an increment of 1% until a significant increase in sample mass (when compared to the baseline drift) was observed, and the RH at which the sample mass showed a significant increase was equal to its DRH. Each measurement was repeated at least three times, and the average value and standard deviation were reported. At each RH the sample was considered to reach equilibrium with the environment when its mass change was <0.1% within 30 min, and RH was changed to the next value only after the sample mass was stabilized. The time to reach a new equilibrium varied with compounds and largely depended on the dry sample mass, i.e. a sample with larger dry mass would took longer to reach the equilibrium.

3 Results and discussion

3.1 Hygroscopicity of nitrates and chlorides

3.1.1 DRH at different temperature

First we investigated the effect of temperature on the DRH of $Ca(NO_3)_2 \cdot 4H_2O$, $Mg(NO_3)_2 \cdot 6H_2O$ and $MgCl_2 \cdot 6H_2O$, which are the most stable forms of corresponding salts for the temperature range (5-30 ^oC) considered in this work (Kelly and Wexler, 2005). Figure 1a shows the change of RH and normalized sample mass as a function of time in an experiment to measure the DRH of $Mg(NO_3)_2 \cdot 6H_2O$ at 25 ^oC. Abrupt and significant increase in sample mass was observed when RH was increased from 52 to 53%, suggesting that the deliquescence occurred between 52 and 53% RH. Therefore, its DRH was measured to be 52.5±0.5 %. It should be noted that the mass change was >15% when RH was increased from 52 to 53%, as shown in Figure 1a; such a large mass increase cannot be solely caused by water adsorption. The continuous but small decrease in sample mass (about 1% in total) with time (around 500-1000 min) before deliquescence took place, as shown in Figure 1a, was likely caused by desorption of residual water contained by the sample under investigation.

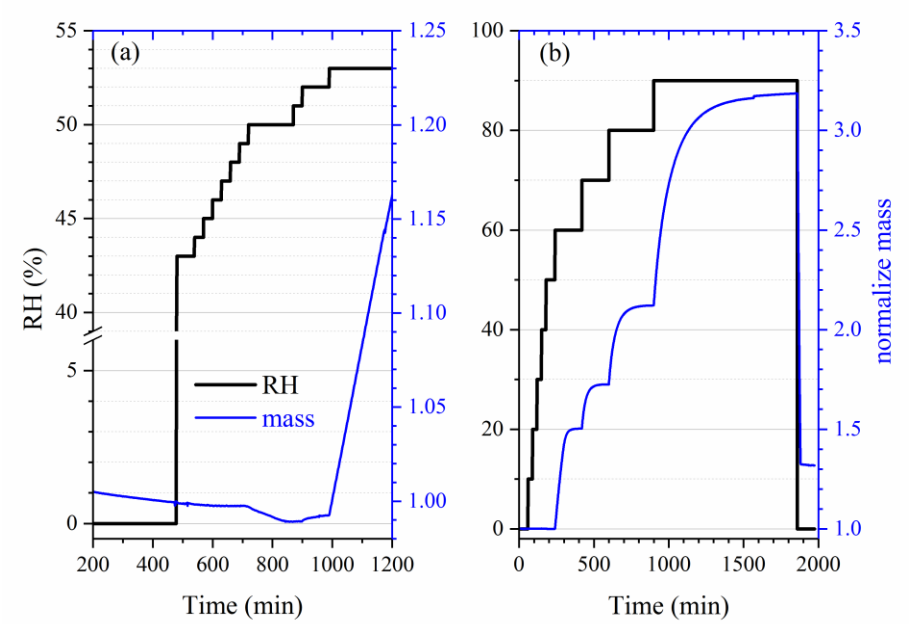

Figure 1. Change of normalized sample mass (blue curve, right *y*-axis) and RH (black curve, left *y*-axis) as a function of time. (a) A typical experiment conducted to measure the DRH; (b) A typical experiment conducted to measure mass hygroscopic growth factors. In the two experiments shown here, $Mg(NO_3)_2 \cdot 6H_2O$ was investigated at 25 ^oC.

Table 1 summarizes our measured DRH of $Ca(NO_3)_2 \cdot 4H_2O$, $Mg(NO_3)_2 \cdot 6H_2O$ and $MgCl_2 \cdot 6H_2O$ as a function of temperature (5-30 ^oC). DRH values show a strong dependence on temperature for $Ca(NO_3)_2 \cdot 4H_2O$ (decreasing from 60.5% at 5 ^oC to 46.0% at 30 ^oC) and a weaker temperature dependence for $Mg(NO_3)_2 \cdot 6H_2O$ (decreasing from 57.5% at 5 ^oC to 50.5% at 30 ^oC); in contrast, the DRH values of $MgCl_2 \cdot 6H_2O$ (31.5-32.5 %) exhibit little variation with temperature (5-30 ^oC). Several previous studies have reported the DRH of $Ca(NO_3)_2 \cdot 4H_2O$, $Mg(NO_3)_2 \cdot 6H_2O$ and $MgCl_2 \cdot 6H_2O$, and their results are compared with our work in the following paragraphs.

Table 1. DRH (in %) of $Ca(NO_3)_2 \cdot 4H_2O$, $Mg(NO_3)_2 \cdot 6H_2O$ and $MgCl_2 \cdot 6H_2O$ measured in this work as a function of temperatures (5-30 °C). Solubility data (mol per kg water) compiled by Kelly and Wexler (2005) was used to calculate solubilities in mol per mol water. All the errors given in this work are standard deviations.

T (°C)	$Ca(NO_3)_2 \cdot 4H_2O$	$Mg(NO_3)_2 \cdot 6H_2O$	$MgCl_2 \cdot 6H_2O$
5	60.5±1.0	57.5±1.0	32.5±1.0
10	58.0±1.0	56.5±1.0	32.5±1.0
15	55.5±1.0	54.5±1.0	32.5±1.0
20	52.5±1.0	53.5±1.0	32.5±1.0
25	49.5±1.0	52.5±1.0	31.5±1.0
30	46.0±1.0	50.5±1.0	31.5±1.0
solubility (mol per kg water)	8.4	4.9	5.84
solubility (A, mol per mol water)	0.1512	0.0882	0.1051
$A \cdot \Delta H_s/R$ (K)	913±59	427±28	--
ΔH_s (kJ mol^{-1})	50.2±3.3	40.3±2.6	--

The $A \cdot \Delta H_s/R$ and ΔH_s values were not estimated for $MgCl_2 \cdot 6H_2O$ because the difference in its measured DRH between 5 and 30 °C was very small or even insignificant. Please refer to Section 3.1.1 for further details.

$Ca(NO_3)_2 \cdot 4H_2O$: RH of air in equilibrium with saturated $Ca(NO_3)_2 \cdot 4H_2O$ solutions, i.e. the DRH values of $Ca(NO_3)_2 \cdot 4H_2O$, were measured to be 55.9, 55.4, 50.5 and 46.7% at 15, 20, 25 and 30 °C (Adams and Merz, 1929), and the absolute differences between DRH reported by Adams and Merz (1929) and those measured in our work are <3%. The water vapor pressures of saturated $Ca(NO_3)_2 \cdot 4H_2O$ solutions were measured to be 0.693, 0.920, 1.253, 1.591 and 1.986 kPa at 10, 15, 20, 25 and 30 °C (Apelblat, 1992), corresponding to DRH of 56, 54, 54, 50 and 47%, respectively; therefore, the absolute difference between DRH measured in our work and those derived from Apelblat (1992) are <2%. In another study (Al-Abadleh et al., 2003), RH over the saturated

$Ca(NO_3)_2 \cdot 4H_2O$ solution was measured to be 57±5% at room temperature, also in broad consistence with our work (49.5±1.0% at 25 °C).

$Mg(NO_3)_2 \cdot 6H_2O$: Water vapor pressures of saturated $Mg(NO_3)_2 \cdot 6H_2O$ solutions were determined to be 0.737, 1.017, 1.390, 1.813 and 2.306 kPa at 10, 15, 20, 25 and 30 °C (Apelblat, 1992), giving DRH of 60, 60, 59, 57 and 54% at corresponding temperatures. The vapor pressure of saturated $Mg(NO_3)_2 \cdot 6H_2O$ solutions at 25 °C were reported to be 1.674 and 1.666 kPa by another two studies (Biggs et al., 1955; Robinson and Stokes, 1959), corresponding to DRH of ~53%. In addition, the water activity of the saturated $Mg(NO_3)_2$ solution was measured to be 0.528 at 25 °C (Rard et al., 2004), also suggesting a DRH value of ~53%; similarly, RH over the saturated $Mg(NO_3)_2$ solution was reported to be ~53% at 22-24 °C (Li et al., 2008b). Al-Abadleh and Grassian (2003) investigated the phase transition of the $Mg(NO_3)_2 \cdot 6H_2O$ film, and its DRH was determined to be 49-54% at 23 °C. As shown in Table 1, DRH measured in our work agree very well with those reported by most of previous studies (Biggs et al., 1955; Robinson and Stokes, 1959; Al-Abadleh and Grassian, 2003; Rard et al., 2004), but are always 3-5% lower than those derived from Apelblat (1992). This may imply that water vapor pressure measurements by Apelblat (1992) could have unknown systematical errors.

$MgCl_2 \cdot 6H_2O$: Kelly and Wexler (2005) calculated DRH of $MgCl_2 \cdot 6H_2O$ from vapor pressures of saturated $MgCl_2 \cdot 6H_2O$ solutions measured by previous work, and found that DRH values were in the range of 33-34% for temperatures at 0-40 °C. In addition, water activity of the saturated $MgCl_2$ solution was reported to be 0.3278 at 25 °C (Rard and Miller, 1981), corresponding to a DRH value of ~33% for $MgCl_2 \cdot 6H_2O$. The DRH values of $MgCl_2 \cdot 6H_2O$ measured in our work, as summarized in Table 1, show excellent agreement with those reported by previous work (Rard and Miller, 1981; Kelly and Wexler, 2005). Phase transition and

deliquescence behavior of $CaCl_2 \cdot 6H_2O$ were also investigated in our work and found to be very complex, and the result will be discussed in Section 3.1.3.

Temperature in the troposphere varies from ~200 to >300 K, and it is thus warranted to explore the effects of temperature on hygroscopic properties of atmospherically relevant particles. The dependence of DRH on temperature can usually be approximated by the Clausius-Clapeyron equation (Wexler and Seinfeld, 1991; Seinfeld and Pandis, 2006; Jia et al., 2018):

$$\ln[DRH(T)] = \ln[\mathrm{DRH}(298)] + \frac{A \cdot \Delta H_s}{R}\left(\frac{1}{T} - \frac{1}{298}\right) \quad (2)$$

where T is temperature (K), DRH(T) and DRH(298) are the DRH at T and 298 K, R is the gas constant (8.314 J mol^{-1} K^{-1}), and ΔH_s is the enthalpy of dissolution (J mol^{-1}). The dimensionless constant, A, is numerically equal to the water solubility of the salt under investigation in the unit of mol per mol water. Figure 2 shows the dependence of DRH values on temperature for $Ca(NO_3)_2 \cdot 4H_2O$ and $Mg(NO_3)_2 \cdot 6H_2O$, confirming that Eq. (2) can indeed approximate the temperature dependence. The slope, which is equal to $A \cdot \Delta H_s/R$, was determined to be 913±59 K for $Ca(NO_3)_2 \cdot 4H_2O$ and 427±28 K for $Mg(NO_3)_2 \cdot 6H_2O$, and thus ΔH_s was derived to be 50.2±3.3 kJ mol^{-1} for $Ca(NO_3)_2 \cdot 4H_2O$ and 40.3±2.6 kJ mol^{-1} for $Mg(NO_3)_2 \cdot 6H_2O$. It should be noted that for Eq. (2) to be valid, both the enthalpy of dissolution and the water solubility are assumed to be constant for the temperature range considered. The variation of DRH with temperature (5-30 ºC) was very small and even insignificant for $MgCl_2 \cdot 6H_2O$; as a result, we did not attempt to estimate the ΔH_s values for $MgCl_2 \cdot 6H_2O$ since such estimation would have large errors.

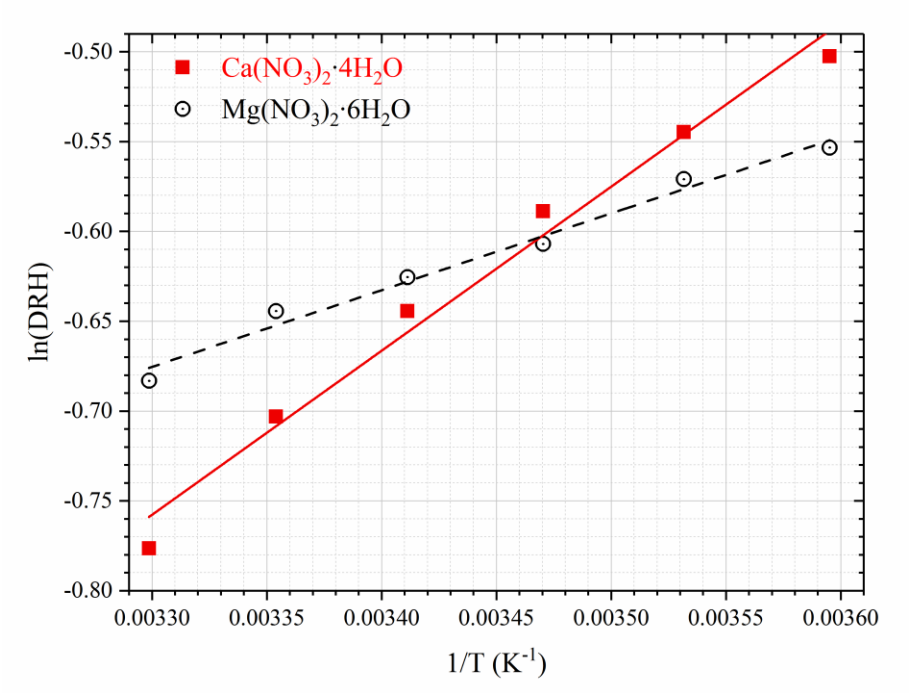

Figure 2. Dependence of DRH on temperature for $Ca(NO_3)_2 \cdot 4H_2O$ and $Mg(NO_3)_2 \cdot 6H_2O$.

3.1.2 Water-to-solute ratios as a function of RH

The change of sample mass with RH (0-90%) was measured at 5 and 25 °C for $Ca(NO_3)_2 \cdot 4H_2O$, $Mg(NO_3)_2 \cdot 6H_2O$ and $MgCl_2 \cdot 6H_2O$, using the vapor sorption analyzer. The mass change, relative to that at 0% RH, can be used to calculate water-to-solute ratios (WSR, defined in this work as the molar ratio of H_2O to Ca^{2+} or Mg^{2+}) for deliquesced samples. Small changes in m/m_0 (typically <2%) were observed for some compounds (as shown in Tables 2 and 6) when RH was below corresponding DRH values, mainly due to water adsorption/desorption and baseline drift. As summarized in Table 2, decrease in temperature would lead to increase in WSR at a given RH: at 90% RH for example, WSR were determined to be 28.78±0.20 at 25 °C and 31.80±0.96 at 5 °C for $Ca(NO_3)_2 \cdot 4H_2O$, 36.87±0.23 at 25 °C and 41.40±1.36 at 5 °C for $Mg(NO_3)_2 \cdot 6H_2O$, and 36.26±1.76 at 25 °C and 39.55±2.43 at 5 °C for $MgCl_2 \cdot 6H_2O$, respectively. As discussed in Section 3.1.1, the enthalpies of dissolution (ΔH_s) are negative for these compounds, suggesting that their

dissolution processes in water are exothermic; therefore, dissolution is favored at lower temperatures and at a given RH, decrease in temperature would lead to increase in WSR in the aqueous solutions. Several previous studies have measured RH over aqueous $Ca(NO_3)_2$, $Mg(NO_3)_2$ and $MgCl_2$ solutions at given concentrations, and their results are compared with our work, as discussed below.

Table 2. Mass growth factors (m/m_0, defined as the ratio of sample mass at a given RH to that at 0% RH) and water-to-solute ratios (WSR) as a function of RH (0-90%) at 25 and 5 °C for $Ca(NO_3)_2{\cdot}4H_2O$, $Mg(NO_3)_2{\cdot}6H_2O$ and $MgCl_2{\cdot}6H_2O$. WSR were only calculated for RH exceeding the DRH (i.e. when the sample was deliquesced). All the errors given in this work are standard deviations.

	$Ca(NO_3)_2{\cdot}4H_2O$, 25 °C		$Ca(NO_3)_2{\cdot}4H_2O$, 5 °C	
RH (%)	m/m_0	WSR	m/m_0	WSR
0	1.000±0.001	--	1.000±0.001	--
10	1.000±0.001	--	1.001±0.001	--
20	1.014±0.005	--	1.005±0.003	--
30	1.016±0.007	--	1.005±0.002	--
40	1.017±0.009	--	1.009±0.003	--
50	1.237±0.006	7.10±0.03	1.032±0.005	--
60	1.363±0.008	8.76±0.05	1.041±0.002	--
70	1.550±0.009	11.22±0.06	1.610±0.010	12.00±0.07
80	1.897±0.012	15.77±0.10	1.979±0.027	16.85±0.23
90	2.889±0.020	28.78±0.20	3.119±0.095	31.80±0.96
	$Mg(NO_3)_2{\cdot}6H_2O$, 25 °C		$Mg(NO_3)_2{\cdot}6H_2O$, 5 °C	
RH (%)	m/m_0	WSR	m/m_0	WSR
0	1.000±0.001	--	1.000±0.001	--
10	1.000±0.001	--	1.000±0.001	--
20	1.000±0.001	--	1.000±0.001	--

30	1.001±0.001	--	1.000±0.001	--
40	1.001±0.001	--	1.000±0.001	--
50	1.000±0.001	--	1.000±0.001	--
60	1.503±0.001	13.15±0.01	1.539±0.003	13.67±0.03
70	1.724±0.001	16.30±0.01	1.773±0.007	16.99±0.07
80	2.121±0.001	21.94±0.01	2.203±0.021	23.11±0.22
90	3.171±0.029	36.87±0.23	3.489±0.114	41.40±1.36

	$MgCl_2 \cdot 6H_2O$, 25 °C		$MgCl_2 \cdot 6H_2O$, 5 °C	
RH (%)	m/m_0	WSR	m/m_0	WSR
0	1.000±0.001	--	1.000±0.001	--
10	1.000±0.001	--	1.000±0.001	--
20	1.000±0.001	--	1.000±0.001	--
30	1.001±0.001	--	1.000±0.001	--
40	1.344±0.057	9.89±0.42	1.327±0.082	9.69±0.60
50	1.489±0.062	11.52±0.48	1.473±0.090	11.34±0.69
60	1.677±0.072	13.65±0.58	1.667±0.100	13.52±0.82
70	1.951±0.084	16.74±0.72	1.950±0.117	16.72±1.00
80	2.433±0.117	22.18±1.06	2.465±0.148	22.54±1.35
90	3.681±0.178	36.26±1.76	3.972±0.244	39.55±2.43

$Ca(NO_3)_2$: Water activities of $Ca(NO_3)_2$ solutions at 25 °C were measured to be 0.904, 0.812 and 0.712 when the concentrations were 2.0, 3.5 and 5.0 mol kg^{-1}, respectively (El Guendouzi and Marouani, 2003). Since water activity of a solution is equal to the RH of air in equilibrium with the solution, it can be derived that the molality concentrations of $Ca(NO_3)_2$ solution were 2.0, 3.5 and 5.0 mol kg^{-1} when RH was 71.2, 81.2 and 90.4%; in other words, WSR were found to be 11.1, 15.9 and 27.8 at 71.2, 81.2 and 90.4 % RH, respectively (El Guendouzi and Marouani, 2003). As shown in Table 2, in our work WSR were determined to be 11.22±0.06, 15.77±0.10 and 28.78±0.20 at 70, 80 and 90% RH for $Ca(NO_3)_2$ solutions at the same temperature, suggesting good agreement with El Guendouzi and Marouani (2003).

$Mg(NO_3)_2$: Water activities of $Mg(NO_3)_2$ solutions were reported to be 0.897, 0.812 and 0.702 when the concentrations of the bulk solutions were 1.6, 2.5 and 3.5 mol kg^{-1} at 25 °C, respectively (Rard et al., 2004); this means that WSR were equal to 15.9, 22.2 and 34.7 at 70.2, 81.2 and 89.7% RH. Ha and Chan (1999) fitted their measured water activities of $Mg(NO_3)_2$ as a function of molality concentration at 20-24 °C with a polynomial equation, and WSR were derived to be 12.93, 16.12, 21.50 and 36.09 at 60, 70, 80 and 90% RH. As shown in Table 2, WSR were measured to be 13.15±0.01, 16.30±0.01, 21.94±0.01 and 36.87±0.23 at 60, 70, 80 and 90% RH for deliquesced $Mg(NO_3)_2$ at 25 °C. Therefore, it can be concluded that for WSR of $Mg(NO_3)_2$ solutions at ~25 °C, our work shows good agreement with the two previous studies (Ha and Chan, 1999; Rard et al., 2004).

$MgCl_2$: Water activities of $MgCl_2$ solutions were reported to be 0.909, 0.800, 0.692, 0.491 and 0.408 when the concentrations were 1.4, 2.4, 3.2, 4.6 and 5.2 mol kg^{-1} (Rard and Miller, 1981), i.e. WSR were equal to 10.7, 12.1, 17.4, 23.1 and 39.7 at 40.8, 49.1, 69.2, 80.0 and 90.9% RH. In another work (Ha and Chan, 1999), an electrodynamic balance was used to investigate hygroscopic growth of $MgCl_2$ particles at 20-24 °C, and the measured molality concentrations of $MgCl_2$ solutions as a function of water activity were fitted by a polynomial equation; it can be derived from Ha and Chen (1999) that WSR were equal to 10.65, 12.34, 14.29, 17.04, 22.24 and 34.78 when RH were 40, 50, 60, 70, 80 and 90%, respectively. WSR measured in our work, as listed in Table 2, are 9.89±0.42, 11.52±0.48, 1.677±0.072, 16.74±0.72, 22.18±1.06 and 36.26±1.76 at 40, 50, 60, 70, 80 and 90% RH. As a result, our work agrees well with the two previous studies (Rard and Miller, 1981; Ha and Chan, 1999) for WSR of $MgCl_2$ solutions as a function of RH at ~25 °C.

3.1.3 Phase transition of $CaCl_2 \cdot xH_2O$

The change in sample mass of $CaCl_2 \cdot 6H_2O$ with RH was also investigated at 25 °C. As shown in Figure 3, when dried at 0% RH, the sample mass was reduced by 1/3 (from ~1.5 to ~1.0), and it is speculated that $CaCl_2 \cdot 6H_2O$ was converted to $CaCl_2 \cdot 2H_2O$. When RH was increased to 10%, no significant increase in sample mass was observed. As RH was further increased to 20%, the sample mass was increased by 48±7 %; this may indicate that $CaCl_2 \cdot 2H_2O$ was converted to $CaCl_2 \cdot 6H_2O$, as the ratio of molar mass of $CaCl_2 \cdot 6H_2O$ (219 g mol^{-1}) to $CaCl_2 \cdot 2H_2O$ (147 g mol^{-1}) is 1.49, approximately equal to the ratio of sample mass at 20% RH to that at 10% RH. Further increase in RH to 30% would lead to additional increase in sample mass, implying the deliquescence of the sample and the formation of an aqueous $CaCl_2$ solution.

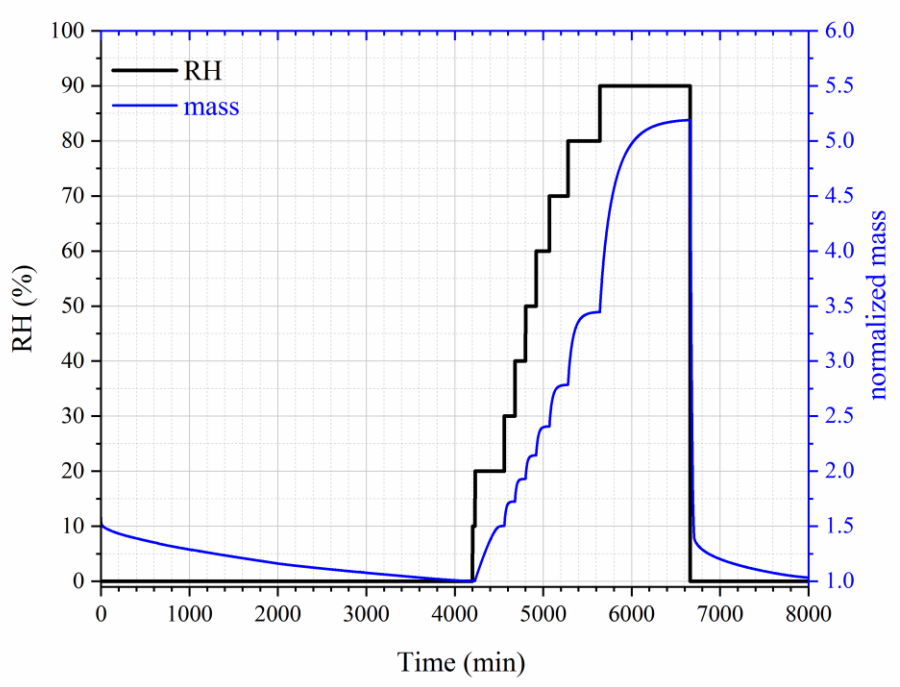

Figure 3. Change of normalized sample mass (blue curve, right *y*-axis) and RH (black curve, left *y*-axis) as a function of time for $CaCl_2 \cdot xH_2O$ at 25 °C.

Assuming that $CaCl_2 \cdot 6H_2O$ was converted to $CaCl_2 \cdot 2H_2O$ after being dried at 0% RH, we could use the change of sample mass as a function of RH to calculate WSR (defined as molar ratio of H_2O to Ca^{2+}), and the results are listed in Table 3. Please note that we did not calculate WSR at 20% RH, since it is speculated that the significant mass increase at 20% RH was caused by the transformation of $CaCl_2 \cdot 2H_2O$ to $CaCl_2 \cdot 6H_2O$, as mentioned above. Water activities of aqueous $CaCl_2$ solutions as a function of molality concentration reported in a previous study (Rard et al., 1977) were used to calculate WSR as a function of RH, and the results are also included in Table 3 for comparison. As evident from Table 3, at same/similar RH, WSR measured in our work are in good agreement with those derived from Rard et al. (1977), supporting our assertion that $CaCl_2 \cdot 6H_2O$ was converted to $CaCl_2 \cdot 2H_2O$ after being dried at 0% RH. In fact, theoretical calculations (Kelly and Wexler, 2005) and experimental measurements (Gough et al., 2016) both suggested that when RH is gradually increased, solid-solid phase transition from $CaCl_2 \cdot 2H_2O$ to $CaCl_2 \cdot 6H_2O$ would occur before deliquescence takes place.

Table 3. Mass growth factors (m/m_0, defined as the ratio of sample mass at a given RH to that at 0% RH) and water-to-solute ratios (WSR) as a function of RH (0-90%) at 25 °C for $CaCl_2 \cdot xH_2O$. WSR derived from RH over aqueous $CaCl_2$ solutions as a function of concentration (mol kg^{-1}) at 25 °C (Rard et al., 1977) are also included for comparison. All the errors given in this work are standard deviations.

our work			Rard et al., 1977		
RH (%)	m/m_0	WSR	RH (%)	molality	WSR
0	1.000±0.001	--	--	--	--
10	1.000±0.001	--	--	--	--
20	1.448±0.072	--	--	--	--
30	1.724±0.007	7.97±0.03	31.2	7.0	7.94

40	1.929±0.008	9.64±0.04	39.2	6.0	9.26
50	2.144±0.010	11.40±0.05	49.9	5.0	11.11
60	2.408±0.012	13.55±0.07	--	--	--
70	2.786±0.015	16.64±0.09	70.1	3.4	16.34
80	3.448±0.020	22.05±0.13	79.8	2.6	21.37
90	5.194±0.030	36.30±0.21	89.9	1.6	37.72

Additional experiments, in which RH was stepwise increased from 0% with an increment of 1% per step, were carried out in attempt to measure the DRH of $CaCl_2 \cdot xH_2O$ at 25 ^oC. In all of these experiments, $CaCl_2 \cdot 6H_2O$ was always transformed to $CaCl_2 \cdot 2H_2O$ after being dried at 0% RH. In some of these experiments the deliquescence took place at RH of ~28.5%, which is consistent with the DRH of $CaCl_2 \cdot 6H_2O$ reported in the literature (Kelly and Wexler, 2005), suggesting that $CaCl_2 \cdot 2H_2O$ was first transformed to $CaCl_2 \cdot 6H_2O$ prior to deliquescence; however, in some experiments the deliquescence occurred at RH of ~18.5%, corresponding to the DRH of $CaCl_2 \cdot 2H_2O$ reported previously (Kelly and Wexler, 2005), implying that $CaCl_2 \cdot 2H_2O$ was deliquesced without being transformed to $CaCl_2 \cdot 6H_2O$. The dual deliquescence processes, i.e. 1) transformation of $CaCl_2 \cdot 2H_2O$ to $CaCl_2 \cdot 6H_2O$ prior to deliquescence and 2) direct deliquescence of $CaCl_2 \cdot 2H_2O$, were also observed using Raman spectroscopy at low temperatures (223-273 K) (Gough et al., 2016). It seems that the competition of these two mechanisms are both thermodynamically and kinetically dependent. Since phase transitions of $CaCl_2$ are not only important for atmospheric aerosols but may also play a role in the existence of liquid water in some hyperarid environments (Gough et al., 2016), further investigation is being carried out by combining the vapor sorption analyzer technique with vibrational spectroscopy.

3.1.4 Hygroscopic growth of aerosol particles

Hygroscopic growth factors (GF), which were measured using H-TDMA at room temperature, are displayed in Figure 4 for $Ca(NO_3)_2$, $CaCl_2$, $Mg(NO_3)_2$ and $MgCl_2$ aerosols, and the results are also compiled in Table 4. It was found in our work that all the four types of aerosols exhibit high hygroscopicity, with GF at 90% RH being around 1.7 or larger. In addition, all the four types of aerosol particles, instead of having distinct solid-liquid phase transitions, showed significant hygroscopic growth at very low RH (as low as 10%), and their GF increased continuously with RH. This phenomenon is due to the fact that these aerosol particles, generated by drying aqueous droplets, were likely to be amorphous. It was also observed in previous work that some types of particles generated by drying aqueous droplets would be amorphous, such as $Ca(NO_3)_2$ (Tang and Fung, 1997; Gibson et al., 2006; Jing et al., 2018), $Mg(NO_3)_2$ (Zhang et al., 2004; Gibson et al., 2006; Li et al., 2008a), $CaCl_2$ (Park et al., 2009; Tobo et al., 2009) and $MgCl_2$ (Cziczo and Abbatt, 2000; Park et al., 2009).

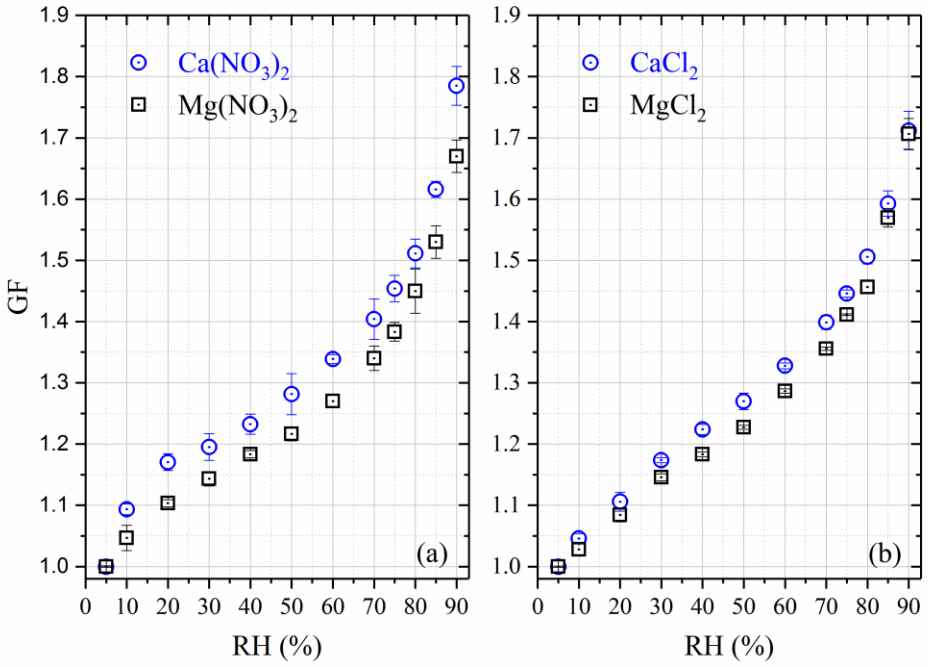

Figure 4. Hygroscopic growth factors (GF) of aerosol particles as a function of RH measured using H-TDMA. (a): $Ca(NO_3)_2$ and $Mg(NO_3)_2$; (b) $CaCl_2$ and $MgCl_2$.

$Ca(NO_3)_2$ and $Mg(NO_3)_2$ aerosols: Two previous studies (Gibson et al., 2006; Jing et al., 2018) employed H-TDMA to examine the hygroscopic growth of 100 nm $Ca(NO_3)_2$ aerosol particles at room temperature. GF were determined to be 1.51 at 80% RH and ~1.77 at 85% RH by Gibson et al. (2008). It should be pointed out that though the DMA-selected dry particle diameters were 100 nm for $Ca(NO_3)_2$ and $Mg(NO_3)_2$ aerosols, the dry diameters used by Gibson et al. (2006) were 89 nm for $Ca(NO_3)_2$ and 77 nm for $Mg(NO_3)_2$, being extrapolated to 0% RH using the theoretical growth curve based on the Köhler theory. The Köhler theory is based on assumption of solution ideality, and thus may not be applicable to highly concentrated aerosol droplets at very low RH (Seinfeld and Pandis, 2006). If the dry diameter selected using the DMA (i.e. 100 nm) was used in GF calculation, GF reported by Gibson et al. (2006) would be ~1.34 at 80% RH and ~1.58 at 85% RH; compared with our results (1.51±0.02 at 80% RH and 1.62±0.01 at 85% RH), GF reported by Gibson et al. (2006) are ~11% smaller at 80% RH and only ~3% smaller at 85%. In the second study (Jing et al., 2018), GF were determined to be 1.56 at 80% RH and 1.89 at 90% RH; compared with our results (1.51±0.02 at 80% RH and 1.79±0.03 at 90% RH), GF reported by Jing et al. (2018) were ~3% larger at 80% RH and ~6% larger at 90% RH. Overall, our results show reasonably good agreement with the two previous studies (Gibson et al., 2006; Jing et al., 2018).

Table 4. Hygroscopic growth factors (GF) of $Ca(NO_3)_2$, $CaCl_2$, $Mg(NO_3)_2$ and $MgCl_2$ aerosol particles measured at room temperature using H-TDMA. The absolute uncertainties in RH were estimated to be within ±2%. All the errors given in this work are standard deviations.

RH (%)	$Ca(NO_3)_2$	$CaCl_2$	$Mg(NO_3)_2$	$MgCl_2$

<5	1.00±0.01	1.00±0.01	1.00±0.01	1.00±0.01
10	1.09±0.01	1.05±0.01	1.05±0.02	1.03±0.01
20	1.17±0.02	1.11±0.02	1.10±0.01	1.08±0.01
30	1.20±0.02	1.17±0.01	1.41±0.01	1.15±0.01
40	1.23±0.02	1.22±0.01	1.18±0.01	1.18±0.01
50	1.28±0.03	1.27±0.01	1.22±0.01	1.23±0.01
60	1.34±0.01	1.33±0.01	1.27±0.01	1.29±0.01
70	1.40±0.03	1.40±0.01	1.34±0.02	1.36±0.01
75	1.45±0.02	1.45±0.01	1.38±0.02	1.41±0.01
80	1.51±0.02	1.51±0.01	1.45±0.04	1.46±0.01
85	1.62±0.01	1.59±0.02	1.53±0.03	1.57±0.02
90	1.79±0.03	1.71±0.03	1.67±0.03	1.71±0.03

To our knowledge, only one previous study investigated the hygroscopic growth of $Mg(NO_3)_2$ aerosol (100 nm) using the H-TDMA (Gibson et al., 2006), and GF was measured to be 1.94±0.02 at 83% RH. As stated above, the theoretical extrapolated diameter (77 nm) at 0% RH, instead of the dry diameter (100 nm) selected using the DMA, were used as the dry diameter to calculate their reported GF (Gibson et al., 2006). If the DMA-selected dry diameter (100 nm) was used in calculation, the GF reported by Gibson et al. (2006) would be ~1.49 at 83% RH; for comparison, in our work GF were determined to be 1.45±0.04 and 1.53±0.03 at 80 and 85% RH, suggesting good agreement between the two studies if the DMA-selected dry diameter was used to calculate GF reported by Gibson et al. (2006).

$CaCl_2$ and $MgCl_2$ aerosols: Hygroscopic growth of $CaCl_2$ and $MgCl_2$ aerosol particles was explored using a H-TDMA (Park et al., 2009), and as far as we know, this was the only study which reported the H-TDMA measured hygroscopic growth factors of the two aerosols. Three dry diameters (20, 30 and 50 nm) were used for $CaCl_2$ and $MgCl_2$ aerosol particles (Park et al., 2009), and no significant size dependence of their hygroscopic properties was observed. GF were

measured to be around 1.27, 1.38, 1.48 and 1.59 at 60, 75, 80 and 90 % RH for $CaCl_2$ (Park et al., 2009). For comparison, GF were determined to be 1.33±0.01, 1.45±0.01, 1.51±0.01 and 1.71±0.03 at 60, 75, 80 and 90 %, slightly larger than those reported by Park et al. (2009), and the differences were found to be <7%.

At 50, 70, 80, 85 and 90% RH, GF of $MgCl_2$ aerosol were measured to be about 1.17, 1.29, 1.47, 1.59 and 1.79 by Park et al. (2009) and 1.23±0.01, 1.36±0.01, 1.46±0.01, 1.57±0.02 and 1.71±0.03 in our work. The differences did not exceed 6%, suggesting good agreement between the two studies. Microscopy was used to investigate the hygroscopic growth of micrometer-size $MgCl_2$ particles deposited on substrates (Gupta et al., 2015), and the ratios of 2-D particle areas, relative to that at <5% RH, were measured to be around 1.65, 1.92, 2.02 and 2.28 at 60, 70, 75 and 80% RH, corresponding to diameter-based GF of approximately 1.28, 1.38, 1.42 and 1.51, respectively. GF of $MgCl_2$ aerosol, as shown in Table 4, were determined to be 1.29±0.01, 1.36±0.01, 1.41±0.01 and 1.46±0.01 at 60, 70, 75 and 80% RH in our work; therefore, the differences between GF reported in our work and those measured by Gupta et al. (2015) were <4%.

Comparison between hygroscopic growth with CCN activities: GF measured using H-TDMA can be used to calculate the single hygroscopicity parameter, κ_{gf}, using Eq. (3a) (Petters and Kreidenweis, 2007; Kreidenweis and Asa-Awuku, 2014; Tang et al., 2016a):

$$\frac{RH}{\exp\left(\frac{A}{d_0 \cdot GF}\right)} = \frac{GF^3 - 1}{GF^3 - (1 - \kappa_{gf})} \qquad (3a)$$

where GF is the growth factor at a given RH; A is a constant which describes the Kelvin effect and is equal to 2.1 nm for a surface tension of 0.072 J m^{-2} (pure water) and temperature of 298.15 K (Tang et al., 2016a). For a dry particle diameter (d_0) of 100 nm, the denominator in the left term

of Eq. (3a) is not larger than 1.02; therefore, the Kelvin effect is negligible and Eq. (3a) can be simplified to Eq. (3b):

$$\mathrm{RH} = \frac{GF^3 - 1}{GF^3 - (1 - \kappa_{gf})} \qquad (3b)$$

Eq. (4) can be derived by rearranging Eq. (3b):

$$\kappa_{gf} = (GF^3 - 1)\frac{1 - RH}{RH} \qquad (4)$$

In our work, GF data at 90% RH were used to derive κ_{gf}, as usually done in many previous studies (Kreidenweis and Asa-Awuku, 2014). The single hygroscopicity parameter, κ_{ccn}, can also be derived from experimental measurements or theoretical calculations of CCN activities (Petters and Kreidenweis, 2007; Kreidenweis and Asa-Awuku, 2014). Ideally aerosol-water interactions under both subsaturation and supersaturation can be described by a constant single hygroscopicity parameter (Petters and Kreidenweis, 2007). Nevertheless, agreement and discrepancies between growth factors derived and CCN activity derived κ have been reported (Petters and Kreidenweis, 2007; Petters et al., 2009; Wex et al., 2009), and several factors can contribute to such discrepancies. First of all, the solutions may not be ideal, and especially aerosol particles under subsaturation may consist of concentrated solutions; secondly, some of the compounds may have limited solubilities. As discussed previously (Petters and Kreidenweis, 2007; Prenni et al., 2007), both factors would lead to lower κ_{gf}, compared to κ_{ccn}. The effect of reduced surface tension, compared to pure water, should be negligible for the eight types of aerosol particles considered in our work, since none of the compounds are known to be surface-active.

Comparison between κ_{gf} determined in our work and κ_{ccn} measured in previous studies is summarized in Table 5 and discussed below for $Ca(NO_3)_2$, $CaCl_2$, $Mg(NO_3)_2$ and $MgCl_2$ aerosols. In previous work which measured CCN activities (Sullivan et al., 2009; Tang et al., 2015; Gaston

et al., 2017), the dry particle diameters used were typically in the range of 50-125 nm. The uncertainties in our derived κ_{gf} have taken into account the uncertainties in measured GF at 90% RH.

Table 5. Comparison between κ_{gf} measured in our work and κ_{ccn} measured in previous studies.

aerosol	κ_{gf} (this work)	κ_{ccn} (previous studies)
$Ca(NO_3)_2$	0.49-0.56	0.44-0.64 (Sullivan et al., 2009) 0.57-0.59 (Tang et al., 2015)
$Mg(NO_3)_2$	0.38-0.43	not measured yet
$CaCl_2$	0.42-0.47	0.46-0.58 (Sullivan et al, 2009) 0.51-0.54 (Tang et al, 2015)) 0.549-0.561 (Gaston et al., 2017)
$MgCl_2$	0.42-0.47	0.456-0.464 (Gaston et al., 2017)
$Ca(HCOO)_2$	0.28-0.31	0.47-0.52 (Tang et al., 2015)
$Mg(HCOO)_2$	0.40-0.45	not measured yet
$Ca(CH_3COO)_2$	0.09-0.13	0.37-0.47 (Tang et al., 2015)
$Mg(CH_3COO)_2$	0.28-0.29	not measured yet

1) For $Ca(NO_3)_2$ aerosol, κ_{ccn} were measured to be 0.44-0.64 by Sullivan et al. (2009) and 0.57-0.59 by Tang et al. (2015); in our work GF at 90% RH was measured to be 1.79±0.03, giving κ_{gf} of 0.49-0.56, in good agreement with κ_{ccn} reported by the two previous studies (Sullivan et al., 2009; Tang et al., 2015).

2) For $CaCl_2$ aerosol, κ_{ccn} were measured to be 0.46-0.58 by Sullivan et al. (2009), 0.51-0.54 by Tang et al. (2015), and 0.549-0.561 by Gaston et al. (2017). GF at 90% RH was determined to be 1.71±0.03 in present work, giving κ_{gf} of 0.42-0.47, slightly lower than κ_{ccn} values measured previously (Sullivan et al., 2009; Tang et al., 2015; Gaston et al., 2017).

3) In our work, GF was determined to be 1.71±0.03 for $MgCl_2$ at 90% RH, giving κ_{gf} of 0.42-0.47; a previous study (Gaston et al., 2017) measured the CCN activity of $MgCl_2$ aerosol, and κ_{ccn} were determined to be 0.456-0.464, in good agreement with κ_{gf} measured in our work.

4) For $Mg(NO_3)_2$ aerosol, GF and κ_{gf} were determined in our work to be 1.67±0.03 and 0.38-0.43, respectively. To our knowledge, CCN activities of $Mg(NO_3)_2$ aerosol have not been experimentally explored yet, and κ_{ccn} were predicted to be 0.8 for $Mg(NO_3)_2$ and 0.3 for $Mg(NO_3)_2 \cdot 6H_2O$ (Kelly et al., 2007; Kreidenweis and Asa-Awuku, 2014), exhibiting a large variation for the same compound with different hydrate states under dry conditions. These calculations were performed using the Köhler theory, assuming solution ideality (Kelly et al., 2007). As Kelly et al. (2007) pointed out, the hydration states, which are not entirely clear for $Mg(NO_3)_2$ aerosol particles under atmospherically relevant conditions, can have large impacts on their hygroscopicity and CCN activities.

3.2 Hygroscopicity of formates and acetates

3.2.1 DRH and water-to-solute ratios

We measured the mass change of $Ca(HCOO)_2$, $Mg(HCOO)_2 \cdot 2H_2O$ and $Ca(CH_3COO)_2 \cdot H_2O$ samples as a function of RH at 25 ^oC, and found that the sample mass remained essentially constant for all the three compounds when RH was increased from 0 to 90%. Therefore, a series of experiments in which RH was increased to 95% were conducted, and for each compounds three duplicate experiments were carried out. As shown in Figure 5a, when RH was increased from 0 to 95%, a significant while small increase in sample mass (>3%) was observed for $Ca(HCOO)_2$. The average ratio of sample mass at 95% RH to that at 0% RH was determined to be for 1.043±0.018 for $Ca(HCOO)_2$ and 1.028±0.008 for $Mg(HCOO)_2 \cdot 2H_2O$ (not

shown in Figure 5), probably indicating that the DRH values were >95% for both compounds at 25 °C.

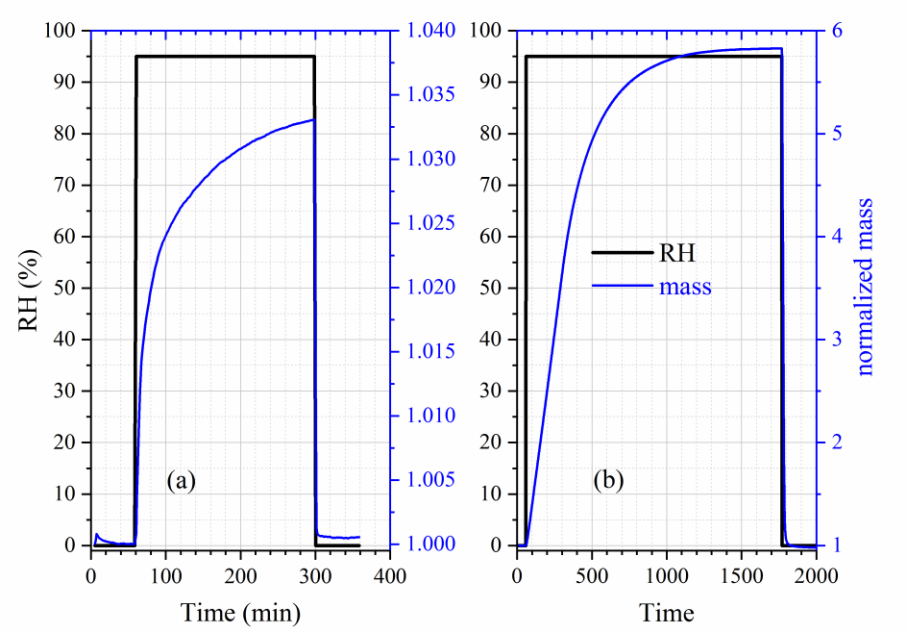

Figure 5. Change of normalized sample mass (blue curve, right *y*-axis) and RH (black curve, left *y*-axis) as a function of time at 25 °C. (a) $Ca(HCOO)_2$; (b) $Ca(CH_3COO)_2 \cdot H_2O$.

When RH was increased from 0 to 95%, large increase in sample mass (almost by a factor of 6), as shown in Figure 6b, was observed for $Ca(CH_3COO)_2 \cdot H_2O$. On average, the ratio of sample mass at 95% RH to that at 0% RH was measured to be 5.849±0.064, corresponding to a WSR (defined as the molar ratio of H_2O to Ca^{2+}) of 48.42±0.53 for the aqueous $Ca(CH_3COO)_2$ solution at 95% RH. This observation suggested that the deliquescence of $Ca(CH_3COO)_2 \cdot H_2O$ at 25 °C occurred between 90 and 95% RH. In further experiments significant increase in sample mass was observed when RH was increased from 90 to 91% for $Ca(CH_3COO)_2 \cdot H_2O$ at 25 °C, suggesting giving a measured DRH of 90.5±1.0 %. The DRH of $Ca(CH_3COO)_2$ and internally mixed $CaCO_3/Ca(CH_3COO)_2$ particles were measured to be 85 and 88% at 5 °C (Ma et al., 2012), using

523 a modified physisorption analyzer. Since in these two studies DRH were measured at different
524 temperatures (25 °C in our work and 5 °C by Ma et al.) and the absolute difference in reported
525 DRH was ~5%, the agreement in reported DRH can be considered to be quite good for
526 $Ca(CH_3COO)_2$.

527 Table 6 summarizes the ratios of sample mass at a given RH to that at 0% RH for
528 $Mg(CH_3COO)_2 \cdot 4H_2O$ as a function of RH at 25°C. Being different from $Ca(HCOO)_2$,
529 $Mg(HCOO)_2 \cdot 2H_2O$ and $Ca(CH_3COO)_2 \cdot H_2O$, large increase in sample mass was observed for
530 $Mg(CH_3COO)_2 \cdot 4H_2O$ when RH was increased from 70 to 80%. This observation suggested that
531 the deliquescence of $Mg(CH_3COO)_2 \cdot 4H_2O$ occurred between 70 and 80% RH. Further
532 experiments were carried out to measure its DRH: significant increase in sample mass occurred
533 when RH was increased from 71 to 72%, giving a measured DRH of 71.5±1.0% at 25 °C. The RH
534 over the saturated $Mg(CH_3COO_2)_2$ solution at ~23 °C was measured to be 65% (Wang et al., 2005),
535 slightly lower than the DRH determined in our work.

536

537 **Table 6.** Mass growth factors (m/m_0, defined as the ratios of sample mass at a given RH to that at
538 0% RH) and water-to-solute ratios (WSR) as a function of RH (0-90%) at 25 °C for
539 $Mg(CH_3COO)_2 \cdot 4H_2O$. WSR are only calculated for RH exceeding the DRH (i.e. when the sample
540 was deliquesced). All the errors given in this work are standard deviations.

RH (%)	0	10	20	30	40
m/m_0	1.000±0.001	1.012±0.021	1.012 ±0.022	1.013 ±0.022	1.013±0.022
WSR	--	--	--	--	--
RH (%)	50	60	70	80	90
m/m_0	1.014±0.023	1.015±0.025	1.033±0.031	2.029±0.013	3.100±0.021
WSR	--	--	--	16.24±0.11	28.97±0.20

541

The ratios of sample mass, relative to that at 0% RH, were measured to be 2.029±0.013 and 3.100±0.021 at 80 and 90% RH, corresponding to WSR of 16.24±0.11 at 80% RH and 28.97±0.20 at 90% RH for aqueous $Mg(CH_3COO)_2$ solutions. A electrodynamic balance coupled to Raman spectroscopy was employed to study the hygroscopic growth of $Mg(CH_3COO)_2$ at ~23 ^oC (Wang et al., 2005), and WSR was determined to be ~15.6 at 80% RH, in good agreement with our work. Ma et al. (2012) found that after heterogeneous reaction with CH_3COOH(g) at 50% RH for 12 h, the hygroscopicity of MgO particles, which was initially rather non-hygroscopic, was substantially increased due to the formation of $Mg(CH_3COO)_2$. The conclusion drawn by Ma et al. (2012) is qualitatively consistent with the results obtained in our work.

Table 5 also reveals that a small increase in sample mass (by ~3%, relative to that at 0% RH) was observed for $Mg(CH_3COO)_2{\cdot}4H_2O$ when RH was increased to 70% before the deliquescence of $Mg(CH_3COO)_2{\cdot}4H_2O$ took place. This could be due to the possibility that $Mg(CH_3COO)_2{\cdot}4H_2O$ samples used in our work may contain a small fraction of amorphous $Mg(CH_3COO)_2$, which would take up some amount of water at RH below the DRH of $Mg(CH_3COO)_2{\cdot}4H_2O$ (Wang et al., 2005; Pang et al., 2015).

3.2.2 Hygroscopic growth of aerosol particles

Figure 6 and Table 6 display hygroscopic growth factors of $Ca(HCOO)_2$, $Mg(HCOO)_2$, $Ca(CH_3COO)_2$ and $Mg(CH_3COO)_2$ aerosols, measured in our work using H-TDMA. To the best of our knowledge, this is the first time that GF of these four types of aerosols have been reported. For $Mg(HCOO)_2$, aerosol particles showed gradual while small growth for RH up to 30%, and further increase in RH led to significant growth; the average GF of $Mg(HCOO)_2$ aerosol at 90% RH was determined to be 1.69±0.03, similar to those for $Mg(NO_3)_2$ (1.67±0.03) and $MgCl_2$ (1.71±0.03) at the same RH. For RH up to 85%, $Ca(HCOO)_2$ aerosol particles exhibited gradual

and small growth; when RH was increased to 90%, abrupt and large growth was observed, with GF being 1.54±0.02, significantly smaller than that for $Mg(HCOO)_2$ aerosol at the same RH. This is distinctively different from what was observed in VSA experiments, in which the mass of $Ca(HCOO)_2$ and $Mg(HCOO)_2{\cdot}2H_2O$ powdered samples was only increased by <5% when RH was increased from 0 to 95%. This difference may be explained by the different states of samples used in these two types of experiments (i. e. crystalline samples in VSA experiments, while likely amorphous aerosol particles in H-TDMA measurements), leading to different hygroscopic behaviors.

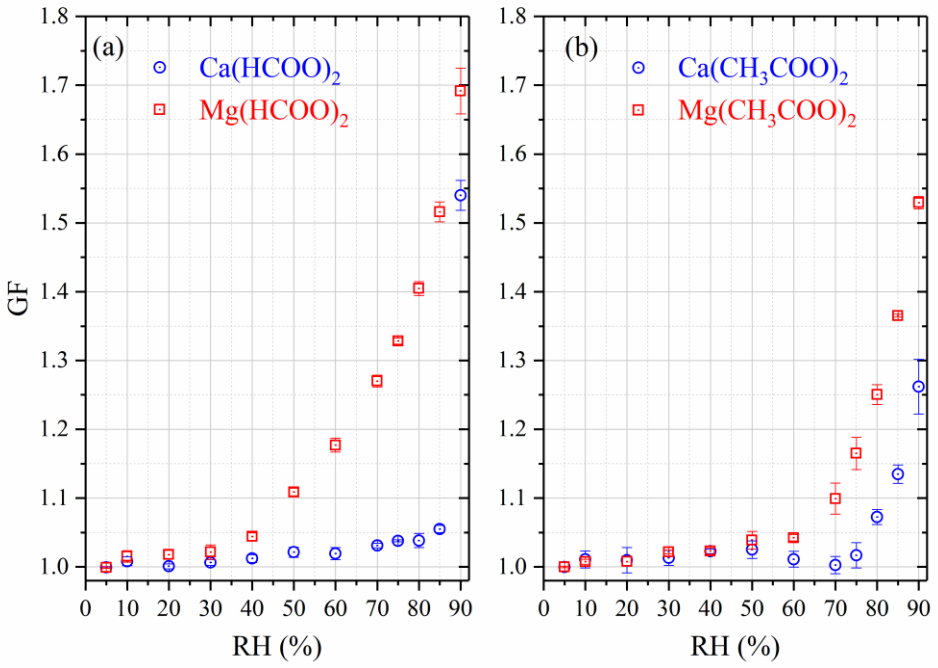

Figure 6. Hygroscopic growth factors (GF) of aerosol particles as a function of RH measured using H-TDMA. (a): $Ca(HCOO)_2$ and $Mg(HCOO)_2$; (b) $Ca(CH_3COO)_2$ and $Mg(CH_3COO)_2$.

As shown in Figure 6b, gradual and small growth was also observed for $Ca(CH_3COO)_2$ and $Mg(CH_3COO)_2$ aerosols at low RH. Fast increase in GF started at about 80% RH for $Ca(CH_3COO)_2$ aerosol, and the GF was determined to be 1.26±0.04 at 90% RH. As discussed in

Section 3.2.1, in VSA experiments no significant increase in sample mass was observed for $Ca(CH_3COO)_2 \cdot H_2O$ when RH was increased from 0 to 90%, being different from H-TDMA results. This difference may again be explained (at least partly) by different states of particles used in these two types of experiments, as mentioned above. Careful inspection of Figure 6b and Table 6 reveals that a small decrease in GF from 1.03±0.01 to 1.00±0.01 for $Ca(CH_3COO)_2$ aerosol when RH was increased from 50 to 70%. Since GF is typically expected to increase with RH, the small decrease in GF (~0.03) for RH between 50 and 70% may reflect the uncertainties in GF measurements (i.e. our H-TDMA measurements cannot resolve a GF difference as small as 0.03).

When RH increased from 0 to 70%, small and gradual growth occurred for $Mg(CH_3COO)_2$ aerosol particles, indicating that these particles may contain some amount of amorphous materials. It was also found in previous work (Li et al., 2008a; Li et al., 2008b) that $Mg(NO_3)_2$ particles generated by drying aqueous droplets were amorphous. Figure 6b reveals that further increase in RH led to large increase in growth factors, and this is largely consistent with the occurrence of deliquescence at ~71.5% RH at 25 ^oC for $Mg(CH_3COO)_2 \cdot 4H_2O$, as mentioned in Section 3.2.1. At 90% RH, GF of $Mg(CH_3COO)_2$ aerosol was determined to be 1.53±0.01, much larger than that for $Ca(CH_3COO)_2$ (1.26±0.04).

At 90% RH, for the four Ca-containing salts considered in our study, nitrate and chloride aerosols have very similar GF (1.79±0.03 versus 1.71±0.03), which are large than that of formate (1.54±0.02), and acetate has the smallest GF (1.26±0.04). For comparison, the variation in GF at 90% RH was found to be considerably smaller (from ~1.53 to ~1.71) for the four Mg-containing salts studied herein.

Table 7. Hygroscopic growth factors of $Ca(HCOO)_2$, $Ca(CH_3COO)_2$, $Mg(HCOO)_2$ and $Mg(CH_3COO)_2$ aerosol particles measured using H-TDMA. The absolute uncertainties in RH were estimated to be within ±2%. All the errors given in this work are standard deviations.

RH (%)	$Ca(HCOO)_2$	$Ca(CH_3COO)_2$	$Mg(HCOO)_2$	$Mg(CH_3COO)_2$
5	1.00±0.01	1.00±0.01	1.00±0.01	1.00±0.01
10	1.01±0.01	1.01±0.01	1.02±0.01	1.01±0.01
20	1.01±0.01	1.01±0.02	1.02±0.01	1.01±0.01
30	1.01±0.01	1.01±0.01	1.02±0.01	1.02±0.01
40	1.01±0.01	1.02±0.01	1.04±0.01	1.02±0.01
50	1.02±0.01	1.03±0.01	1.11±0.01	1.04±0.01
60	1.02±0.01	1.01±0.01	1.18±0.01	1.04±0.01
70	1.03±0.01	1.00±0.01	1.27±0.01	1.10±0.02
75	1.04±0.01	1.02±0.02	1.33±0.01	1.16±0.02
80	1.04±0.01	1.07±0.01	1.41±0.01	1.25±0.01
85	1.01±0.01	1.13±0.01	1.52±0.02	1.37±0.01
90	1.54±0.02	1.26±0.04	1.69±0.03	1.53±0.01

According to Eq. (4), GF measured at 90% RH can be used to calculate κ_{gf}, which were determined to be 0.28-0.31 for $Ca(HCOO)_2$, 0.09-0.13 for $Ca(CH_3COO)_2$, 0.40-0.45 for $Mg(HCOO)_2$, and 0.28-0.29 for $Mg(CH_3COO)_2$. A previous study (Tang et al., 2015) investigated the CCN activities of $Ca(HCOO)_2$ and $Ca(CH_3COO)_2$ aerosols and reported their single hygroscopicity parameters (κ_{ccn}), while the CCN activities of $Mg(HCOO)_2$ and $Mg(CH_3COO)_2$ have not been explored yet. As summarized in Table 5, κ_{ccn} was reported to be 0.47-0.52 for $Ca(HCOO)_2$ (Tang et al., 2015), significantly larger than κ_{gf} (0.28-0.31) determined in our work; for $Ca(CH_3COO)_2$, Tang et al. (2015) reported κ_{ccn} to be in the range of 0.37-0.47, again much larger than κ_{gf} (0.09-0.13) derived from the present work.

As discussed in Section 3.1.4, for $Ca(NO_3)_2$ and $CaCl_2$ aerosols, κ_{gf} derived from H-TDMA experiments in the present work show fairly good agreement with κ_{ccn} derived from CCN activities measured in previous studies (Sullivan et al., 2009; Tang et al., 2015); in contrast, for $Ca(HCOO)_2$ and $Ca(CH_3COO)_2$ aerosols, κ_{gf} derived from our H-TDMA experiments are significantly smaller than κ_{ccn} reported by the previous study (Tang et al., 2015). This can be largely caused by the difference in water solubilities of $Ca(NO_3)_2$, $CaCl_2$, $Ca(HCOO)_2$ and $Ca(CH_3COO)_2$. $Ca(NO_3)_2 \cdot 4H_2O$ and $CaCl_2 \cdot 6H_2O$, with solubilities being 1983 and 1597 g per kg water at 25 ^oC (Kelly and Wexler, 2005), can be considered to be highly soluble; for comparison, the solubilities were reported to be 166 g per kg water for $Ca(HCOO)_2$ at 25 ^oC and 347 g per kg water for $Ca(CH_3COO)_2 \cdot 2H_2O$ at 20 ^oC (Dean, 1973). Due to their limited water solubilities, $Ca(HCOO)_2$ and $Ca(CH_3COO)_2$ aerosol particles may not be fully dissolved at 90% RH in the H-TDMA experiments but would be dissolved to a larger extent (if not completely) for RH >100% in CCN activity measurements (Petters and Kreidenweis, 2008; Kreidenweis and Asa-Awuku, 2014). Therefore, for $Ca(HCOO)_2$ and $Ca(CH_3COO)_2$ aerosols, κ_{gf} derived from H-TDMA measurements would be smaller than κ_{ccn} derived from CCN activity measurements. In fact, the observation that κ_{gf} appeared to be significantly smaller than κ_{ccn}, largely caused by limited water solubilities of compounds under investigation, has been well documented in the literature for laboratory-generated and ambient aerosol particles (Chang et al., 2007; Prenni et al., 2007; Wex et al., 2009; Good et al., 2010; Massoli et al., 2010).

3.3 Discussion

3.3.1 Comparison between H-TDMA and VSA measurements

In this work two complementary techniques were employed to investigate the hygroscopic properties of Ca- and Mg-containing compounds. The mass change of bulk samples was measured

as a function of RH using VSA, and the change in aerosol diameter with RH was determined using H-TDMA. Two major questions can be asked regarding the results obtained using the two different techniques: 1) How can the two types of results be reconciled? 2) What is the atmospheric relevance of each type of results? Below we use $Ca(NO_3)_2$ at room temperature as an example for discussion, and similar conclusions can be drawn for the other seven compounds.

As presented in Section 3.1, at 25 ^oC the deliquescence of $Ca(NO_3)_2 \cdot 4H_2O$ took place at 52-53% RH. In contract, dry $Ca(NO_3)_2$ aerosol particles generated by atomizing aqueous solutions were likely to be amorphous (Tang and Fung, 1997; Al-Abadleh et al., 2003; Gibson et al., 2006); as a result, they exhibited continuous hygroscopic growth with increasing RH with no distinct solid-liquid phase transitions observed. When RH exceed the DRH of $Ca(NO_3)_2 \cdot 4H_2O$, both $Ca(NO_3)_2 \cdot 4H_2O$ bulk samples and $Ca(NO_3)_2$ aerosol particles are expected to deliquesce to form aqueous solutions. To directly link the mass change (measured using VSA) with diameter change (measured using H-TDMA), solution densities, which also vary with RH, are needed. Two important outputs of common aerosol thermodynamic models, such as E-AIM (Clegg et al., 1998) and ISORROPIA II (Fountoukis and Nenes, 2007) are volumes and water-to-solute ratios as a function of RH (above DRH) for aqueous solutions. Water-to-solute ratios and particle diameters were both measured in our work at different RH, and our experimental data, when compared with theoretical calculations, can be used to validate these thermodynamic models.

When RH are lower than the DRH, aerosol particles used in our H-TDMA experiments, instead of bulk samples used in the VSA measurements, are of direct atmospheric relevance, and hence the H-TDMA results should be used in atmospheric implications. There are still some open questions regarding $Ca(NO_3)_2$ aerosol particles (as well as other types of particles investigated in this work) for RH below DRH. What is the phase state of aerosol particles at different RH? Are

they crystalline solid, amorphous solid (glassy), or supersaturated solutions? In this aspect, measurements of particle phase state (Li et al., 2017) of $Ca(NO_3)_2$ and other aerosols considered in our work can shed some light. Furthermore, how do water-to-solute ratios change with RH? This can be answered by determining particle mass as a function of RH for aerosol particles, and techniques are now available for this task (Vlasenko et al., 2017).

3.3.2 Atmospheric implications

Hygroscopicity of carbonate minerals, such as calcite and dolomite, is initially very low and can be largely enhanced due to formation of more hygroscopic materials via heterogeneous reactions during transport (Tang et al., 2016a). Our present work investigated the hygroscopic properties of eight Ca- or Mg-containing compounds which are aging products formed via heterogeneous reactions of carbonate minerals, and revealed that the hygroscopicity of these products is significantly higher than original carbonate minerals. In addition, hygroscopicity was found to differ for different aging products, suggesting that heterogeneous reactions with different trace gases may have distinctive effects on the hygroscopicity of carbonate minerals. For example, the hygroscopicity of $Ca(NO_3)_2$ and $CaCl_2$, formed through heterogeneous reactions with nitrogen oxides and HCl, is much higher than that for $Ca(HCOO)_2$ and $Ca(CH_3COO)_2$, formed via heterogeneous reactions with formic and acidic acids. Our work also observed that significant hygroscopic growth of aerosol particles, such as $Ca(NO_3)_2$ and $CaCl_2$, occurred at RH as low as 10%. This implies that aged carbonate particles can take up significant amount of water even under very low RH, leading to changes in their diameters and morphology and thus impacting their optical properties and direct radiative forcing effects (Pan et al., 2015; Pan et al., 2018).

Large amounts of saline mineral dust are emitted into the atmosphere from dry lake beds (Prospero et al., 2002), but these particles are usually assumed to be nonhygroscopic. Gaston et al.

(2017) found that saline mineral dust particles from different sources exhibit very different CCN activities, and the measured κ_{ccn} varied from <0.01 to >0.8, depending on the abundance of soluble components (e.g., chlorides and sulfates) contained in these particles. Saline mineral dust particles are very likely to have different hygroscopic properties under subsaturation. To understand the hygroscopic growth of saline mineral dust particles, knowledge in hygroscopic growth as well as the abundance of soluble components they contain is needed. Since $CaCl_2$ and $MgCl_2$ have been identified as important components in saline mineral dust, their hygroscopicity data measured in our work will be useful for improving our knowledge in hygroscopic properties of saline mineral dust.

It is conventionally assumed that the hygroscopicity of sea salt is very similar to that of pure NaCl. However, a recent study (Zieger et al., 2017) suggested that the hygroscopic growth factor of sea salt aerosol at 90% RH is 8-15% lower than NaCl aerosol, and this difference is attributed to the presence of $MgCl_2$ and $CaCl_2$ hydrates in sea salt. Growth factors at 90% RH were measured in our work to be ~1.7 for $MgCl_2$ and $CaCl_2$ aerosols, significant lower that for NaCl (2.29-2.46) (Zieger et al., 2017). Therefore, our work provides further experimental results to support the conclusion drawn by Zieger et al., and would help better understand the hygroscopicity of sea salt aerosol.

4. Summary and Conclusion

Ca- and Mg-containing salts, including nitrates, chlorides, formates and acetates, are important components for mineral dust and sea salt aerosols; however, their hygroscopic properties are not well understood yet. In this work, phase transition and hygroscopic growth of eight Ca- or Mg-containing compounds were systematically examined using a vapor sorption analyzer and a humidity-tandem differential mobility analyzer. DRH values decreased from 60.5±1.0% at 5 °C to

46.0±1.0% at 30 °C for $Ca(NO_3)_2 \cdot 4H_2O$ and from 57.5±1.0% at 5 °C to 50.5±1.0% at 30 °C for $Mg(NO_3)_2 \cdot 6H_2O$, both showing negative dependence on temperature, and the dependence of their DRH on temperature can be approximated by the Clausius-Clapeyron equation. No significant dependence of DRH (around 31-33%) on temperature (5-30 °C) was observed for $MgCl_2 \cdot 6H_2O$. $CaCl_2 \cdot 6H_2O$, found to deliquesce at ~28.5% RH at 25 °C, exhibited complex phase transition processes in which $CaCl_2 \cdot 2H_2O$, $CaCl_2 \cdot 6H_2O$ and aqueous $CaCl_2$ solutions were involved. Furthermore, DRH values were determined to be 90.5±1.0% for $Ca(CH_3COO)_2 \cdot H_2O$ and 71.5±1.0% for $Mg(CH_3COO)_2 \cdot 4H_2O$ at 25 °C; for comparison, the sample mass was only increased by <5% for $Ca(HCOO)_2$ and $Mg(HCOO)_2 \cdot 2H_2O$ when RH was increased from 0 to 95%, suggesting that the DRH of these two compounds were >95%.

We have also measured the change of sample mass as a function of RH up to 90% to derive the water-to-solute ratios (WSR) for deliquesced samples. WSR were determined at 25 and 5 °C for deliquesced $Ca(NO_3)_2 \cdot 4H_2O$, $Mg(NO_3)_2 \cdot 6H_2O$ and $MgCl_2 \cdot 6H_2O$ samples, and at 25 °C for deliquesced $CaCl_2 \cdot 6H_2O$ and $Mg(CH_3COO)_2 \cdot 4H_2O$ samples. We found that compared to that at 0% RH, large increases in sample mass only occurred when RH was increased from 90 to 95% for $Ca(CH_3COO)_2 \cdot H_2O$, and the WSR value was determined to be 5.849±0.064 at 95% RH. Besides, deliquescence was not observed even when RH was increased to 95% for $Ca(HCOO)_2$ and $Mg(HCOO)_2 \cdot 2H_2O$, and the ratios of sample mass at 95% to that at 0% RH, were determined to be for 1.043±0.018 for $Ca(HCOO)_2$ and 1.028±0.008 for $Mg(HCOO)_2 \cdot 2H_2O$. Despite that these compounds are important components for tropospheric aerosols, in general they have not been included in widely used aerosol thermodynamic models, such as E-AIM (Clegg et al., 1998) and ISORROPIA II (Fountoukis and Nenes, 2007). The systematical and comprehensive datasets

729 which we have obtained in this work are highly valuable and can be used to validate
730 thermodynamic models if they are extended to include these compounds.

731 In addition, hygroscopic growth of aerosol particles was measured at room temperature for
732 these eight compounds. Being different from solid samples for which the onset of deliquescence
733 was evident, aerosol particles were found to grow in a continuous manner since very low RH (as
734 low as 10%), implying that dry aerosol particles of these eight compounds generated from aqueous
735 droplets were amorphous. Hygroscopic growth factors of aerosol particles at 90% RH were
736 determined to be 1.79±0.03 and 1.67±0.03 for $Ca(NO_3)_2$ and $Mg(NO_3)_2$, 1.71±0.03 for both $CaCl_2$
737 and $MgCl_2$, 1.54±0.02 and 1.69±0.03 for $Ca(HCOO)_2$ and $Mg(HCOO)_2$, and 1.26±0.04 and
738 1.53±0.01 for $Ca(HCOO)_2$ and $Mg(HCOO)_2$. GF at 90% show significant variation (from ~1.26
739 to ~1.79) for the Ca-containing salts investigated here; among them nitrate and chloride have very
740 similar GF (1.79±0.03 versus 1.71±0.03), which are larger than that of formate (1.54±0.02), while
741 acetate has the smallest GF (1.26±0.04). Interestingly, for the four Mg-containing salts considered
742 in this work, the variation in GF at 90 % RH was found to be much smaller (from ~1.53 to ~1.71).

743 GF at 90% RH were used to derive the single hygroscopicity parameters (κ), which were
744 determined to be 0.49-0.56 and 0.38-0.43 for $Ca(NO_3)_2$ and $Mg(NO_3)_2$, 0.42-0.47 for both $CaCl_2$
745 and $MgCl_2$, 0.28-0.31 and 0.40-0.45 for $Ca(HCOO)_2$ and $Mg(HCOO)_2$, and 0.09-0.13 and 0.28-
746 0.29 for $Ca(HCOO)_2$ and $Mg(HCOO)_2$ aerosols, respectively. $Ca(NO_3)_2$ and $CaCl_2$ are very soluble
747 in water, and thus their κ values derived from our H-TDMA experiments are consistent with those
748 reported by previous CCN activity measurements (Sullivan et al., 2009; Tang et al., 2015); on the
749 other hand, due to limited water solubilities, for $Ca(HCOO)_2$ and $Ca(CH_3COO)_2$, κ values derived
750 from our H-TDMA experiments are significantly smaller than those derived from CCN activities
751 in a previous study (Tang et al., 2015). Overall, the present work would significantly improve our

knowledge in the hygroscopic properties of Ca- and Mg-containing salts, and thereby help better understand the physicochemical properties of mineral dust and sea salt aerosols.

Acknowledgement

Financial support provided by the National Natural Science Foundation of China (91744204, 91644106 and 41675120), the Chinese Academy of Sciences international collaborative project (132744KYSB20160036) and the special fund of State Key Joint Laboratory of Environment Simulation and Pollution Control (17K02ESPCP) is acknowledged. Mingjin Tang also would like to thank the CAS Pioneer Hundred Talents program for providing a starting grant. Yujing Tang contributed to this work as an undergraduate intern at Guangzhou Institute of Geochemistry.

References

Adams, J. R., and Merz, A. R.: Hygroscopicity of Fertilizer Materials and Mixtures, Ind. Eng. Chem., 21, 305-307, 1929.

Al-Abadleh, H. A., and Grassian, V. H.: Phase transitions in magnesium nitrate thin films: A transmission FT-IR study of the deliquescence and efflorescence of nitric acid reacted magnesium oxide interfaces, J. Phys. Chem. B, 107, 10829-10839, 2003.

Al-Abadleh, H. A., Krueger, B. J., Ross, J. L., and Grassian, V. H.: Phase transitions in calcium nitrate thin films, Chem. Commun., 2796-2797, 2003.

Apelblat, A.: The vapor pressures of water over saturated solutions of barium chloride, magnesium nitrate, calcium nitrate, potassium carbonate, and zinc sulfate at temperatures from 283 K to 323 K, J. Chem. Thermodyn., 24, 619-626, 1992.

Biggs, A. I., Parton, H. N., and Robinson, R. A.: The Constitution of the Lead Halides in Aqueous Solution, J. Am. Chem. Soc., 77, 5844-5848, 1955.

Chang, R. Y. W., Liu, P. S. K., Leaitch, W. R., and Abbatt, J. P. D.: Comparison between measured and predicted CCN concentrations at Egbert, Ontario: Focus on the organic aerosol fraction at a semi-rural site, Atmos. Environ., 41, 8172-8182, 2007.

Chen, S. Y., Huang, J. P., Kang, L. T., Wang, H., Ma, X. J., He, Y. L., Yuan, T. G., Yang, B., Huang, Z. W., and Zhang, G. L.: Emission, transport, and radiative effects of mineral dust from the Taklimakan and Gobi deserts: comparison of measurements and model results, Atmos. Chem. Phys., 17, 2401-2421, 2017.

Clegg, S. L., Brimblecombe, P., and Wexler, A. S.: Thermodynamic Model of the System H^+–NH_4^+–Na^+–SO_4^{2-}–NO_3^-–Cl^-–H_2O at 298.15 K, J. Phys. Chem. A., 102, 2155-2171, 1998.

Creamean, J. M., Suski, K. J., Rosenfeld, D., Cazorla, A., DeMott, P. J., Sullivan, R. C., White, A. B., Ralph, F. M., Minnis, P., Comstock, J. M., Tomlinson, J. M., and Prather, K. A.: Dust and Biological Aerosols from the Sahara and Asia Influence Precipitation in the Western U.S, Science, 339, 1572-1578, 2013.

Crowley, J. N., Ammann, M., Cox, R. A., Hynes, R. G., Jenkin, M. E., Mellouki, A., Rossi, M. J., Troe, J., and Wallington, T. J.: Evaluated Kinetic and Photochemical Data for Atmospheric Chemistry: Volume V - Heterogeneous Reactions on Solid Substrates, Atmos. Chem. Phys., 10, 9059-9223, 2010.

Cziczo, D. J., and Abbatt, J. P. D.: Infrared observations of the response of NaCl, MgCl2, NH4HSO4, and NH4NO3 aerosols to changes in relative humidity from 298 to 238 K, J. Phys. Chem. A, 104, 2038-2047, 2000.

Cziczo, D. J., Froyd, K. D., Hoose, C., Jensen, E. J., Diao, M., Zondlo, M. A., Smith, J. B., Twohy, C. H., and Murphy, D. M.: Clarifying the Dominant Sources and Mechanisms of Cirrus Cloud Formation, Science, 340, 1320-1324, 2013.
Dean, J. A.: Lange's Handbook on Chemistry (Eleventh Edition), McGraw-Hill, Inc., New York, 1973.
El Guendouzi, M., and Marouani, M.: Water activities and osmotic and activity coefficients of aqueous solutions of nitrates at 25 degrees C by the hygrometric method, J. Solution Chem., 32, 535-546, 2003.
Formenti, P., Rajot, J. L., Desboeufs, K., Saïd, F., Grand, N., Chevaillier, S., and Schmechtig, C.: Airborne observations of mineral dust over western Africa in the summer Monsoon season: spatial and vertical variability of physico-chemical and optical properties, Atmos. Chem. Phys., 11, 6387-6410, 2011.
Formenti, P., Caquineau, S., Desboeufs, K., Klaver, A., Chevaillier, S., Journet, E., and Rajot, J. L.: Mapping the physico-chemical properties of mineral dust in western Africa: mineralogical composition, Atmos. Chem. Phys., 14, 10663-10686, 2014.
Fountoukis, C., and Nenes, A.: ISORROPIA II: a computationally efficient thermodynamic equilibrium model for K^+-Ca^{2+}-Mg^{2+}-NH_4^+-Na^+-SO_4^{2-}-NO_3^--Cl^--H_2O aerosols, Atmos. Chem. Phys., 7, 4639-4659, 2007.
Gaston, C. J., Pratt, K. A., Suski, K. J., May, N. W., Gill, T. E., and Prather, K. A.: Laboratory Studies of the Cloud Droplet Activation Properties and Corresponding Chemistry of Saline Playa Dust, Environ. Sci. Technol., 51, 1348-1356, 2017.
Gibson, E. R., Hudson, P. K., and Grassian, V. H.: Physicochemical properties of nitrate aerosols: Implications for the atmosphere, J. Phys. Chem. A, 110, 11785-11799, 2006.
Ginoux, P., Prospero, J. M., Gill, T. E., Hsu, N. C., and Zhao, M.: Global-scale Attribution of Anthropogenic and Natural Dust Sources and Their Emission Rates Based on MODIS Deep Blue Aerosol Products, Rev. Geophys., 50, RG3005, doi: 3010.1029/2012RG000388, 2012.
Good, N., Topping, D. O., Duplissy, J., Gysel, M., Meyer, N. K., Metzger, A., Turner, S. F., Baltensperger, U., Ristovski, Z., Weingartner, E., Coe, H., and McFiggans, G.: Widening the gap between measurement and modelling of secondary organic aerosol properties?, Atmos. Chem. Phys., 10, 2577-2593, 2010.
Goodman, A. L., Underwood, G. M., and Grassian, V. H.: A Laboratory Study of the Heterogeneous Reaction of Nitric Acid on Calcium Carbonate Particles, J. Geophys. Res.-Atmos., 105, 29053-29064, 2000.
Gough, R. V., Chevrier, V. F., and Tolbert, M. A.: Formation of liquid water at low temperatures via the deliquescence of calcium chloride: Implications for Antarctica and Mars, Planet. Space Sci., 131, 79-87, 2016.
Gu, W. J., Li, Y. J., Tang, M. J., Jia, X. H., Ding, X., Bi, X. H., and Wang, X. M.: Water uptake and hygroscopicity of perchlorates and implications for the existence of liquid water in some hyperarid environments, RSC Adv., 7, 46866-46873, 2017a.
Gu, W. J., Li, Y. J., Zhu, J. X., Jia, X. H., Lin, Q. H., Zhang, G. H., Ding, X., Song, W., Bi, X. H., Wang, X. M., and Tang, M. J.: Investigation of water adsorption and hygroscopicity of atmospherically relevant particles using a commercial vapor sorption analyzer, Atmos. Meas. Tech., 10, 3821-3832, 2017b.
Gupta, D., Eom, H. J., Cho, H. R., and Ro, C. U.: Hygroscopic behavior of NaCl-MgCl2 mixture particles as nascent sea-spray aerosol surrogates and observation of efflorescence during humidification, Atmos. Chem. Phys., 15, 11273-11290, 2015.
Gysel, M., McFiggans, G. B., and Coe, H.: Inversion of tandem differential mobility analyser (TDMA) measurements, J. Aerosol. Sci., 40, 134-151, 2009.
Ha, Z., and Chan, C. K.: The Water Activities of MgCl2, Mg(NO3)2, MgSO4, and Their Mixtures, Aerosol Sci. Technol., 31, 154-169, 1999.
Hatch, C. D., Gough, R. V., and Tolbert, M. A.: Heterogeneous Uptake of the C1 to C4 Organic Acids on a Swelling Clay Mineral, Atmos. Chem. Phys., 7, 4445-4458, 2007.
Hoose, C., and Moehler, O.: Heterogeneous ice nucleation on atmospheric aerosols: a review of results from laboratory experiments, Atmos. Chem. Phys., 12, 9817–9854, 2012.
Jeong, G. Y., and Achterberg, E. P.: Chemistry and mineralogy of clay minerals in Asian and Saharan dusts and the implications for iron supply to the oceans, Atmos. Chem. Phys., 14, 12415-12428, 2014.
Jia, X. H., Gu, W. J., Li, Y. J., Cheng, P., Tang, Y. J., Guo, L. Y., Wang, X. M., and Tang, M. J.: Phase transitions and hygroscopic growth of Mg(ClO4)2, NaClO4, and NaClO4·H2O: implications for the stability of aqueous water in hyperarid environments on Mars and on Earth, ACS Earth Space Chem., 2, 159-167, 2018.
Jickells, T. D., An, Z. S., Andersen, K. K., Baker, A. R., Bergametti, G., Brooks, N., Cao, J. J., Boyd, P. W., Duce, R. A., Hunter, K. A., Kawahata, H., Kubilay, N., laRoche, J., Liss, P. S., Mahowald, N., Prospero, J. M., Ridgwell, A. J., Tegen, I., and Torres, R.: Global Iron Connections between Desert Dust, Ocean Biogeochemistry, and Climate, Science, 308, 67-71, 2005.

Jing, B., Tong, S. R., Liu, Q. F., Li, K., Wang, W. G., Zhang, Y. H., and Ge, M. F.: Hygroscopic behavior of multicomponent organic aerosols and their internal mixtures with ammonium sulfate, Atmos. Chem. Phys., 16, 4101-4118, 2016.
Jing, B., Wang, Z., Tan, F., Guo, Y. C., Tong, S. R., Wang, W. G., Zhang, Y. H., and Ge, M. F.: Hygroscopic behavior of atmospheric aerosols containing nitrate salts and water-soluble organic acids, Atmos. Chem. Phys., 18, 5115-5127, 2018.
Journet, E., Balkanski, Y., and Harrison, S. P.: A New Data Set of Soil Mineralogy for Dust-cycle Modeling, Atmos. Chem. Phys., 14, 3801-3816, 2014.
Kelly, J. T., and Wexler, A. S.: Thermodynamics of carbonates and hydrates related to heterogeneous reactions involving mineral aerosol, J. Geophys. Res.-Atmos, 110, D11201, doi: 11210.11029/12004jd005583, 2005.
Kelly, J. T., Chuang, C. C., and Wexler, A. S.: Influence of dust composition on cloud droplet formation, Atmos. Environ., 41, 2904-2916, 2007.
Khare, P., Kumar, N., Kumari, K. M., and Srivastava, S. S.: Atmospheric formic and acetic acids: An overview, Rev. Geophys., 37, 227-248, 1999.
Kreidenweis, S. M., and Asa-Awuku, A.: 5.13 - Aerosol Hygroscopicity: Particle Water Content and Its Role in Atmospheric Processes, in: Treatise on Geochemistry (Second Edition), edited by: Turekian, K. K., Elsevier, Oxford, 331-361, 2014.
Krueger, B. J., Grassian, V. H., Laskin, A., and Cowin, J. P.: The Transformation of Solid Atmospheric Particles into Liquid Droplets through Heterogeneous Chemistry: Laboratory Insights into the Processing of Calcium Containing Mineral Dust Aerosol in the Troposphere, Geophys. Res. Lett., 30, 1148, doi: 1110.1029/2002gl016563, 2003.
Laskin, A., Iedema, M. J., Ichkovich, A., Graber, E. R., Taraniuk, I., and Rudich, Y.: Direct Observation of Completely Processed Calcium Carbonate Dust Particles, Faraday Discuss., 130, 453-468, 2005.
Lei, T., Zuend, A., Wang, W. G., Zhang, Y. H., and Ge, M. F.: Hygroscopicity of organic compounds from biomass burning and their influence on the water uptake of mixed organic ammonium sulfate aerosols, Atmos. Chem. Phys., 14, 11165-11183, 2014.
Li, H. J., Zhu, T., Zhao, D. F., Zhang, Z. F., and Chen, Z. M.: Kinetics and mechanisms of heterogeneous reaction of NO_2 on $CaCO_3$ surfaces under dry and wet conditions, Atmos. Chem. Phys., 10, 463-474, 2010.
Li, W. J., and Shao, L. Y.: Observation of Nitrate Coatings on Atmospheric Mineral Dust Particles, Atmos. Chem. Phys., 9, 1863-1871, 2009.
Li, X.-H., Zhao, L.-J., Dong, J.-L., Xiao, H.-S., and Zhang, Y.-H.: Confocal Raman Studies of Mg(NO3)2 Aerosol Particles Deposited on a Quartz Substrate: Supersaturated Structures and Complicated Phase Transitions, J. Phys. Chem. B., 112, 5032-5038, 2008a.
Li, X., Dong, J., Xiao, H., Lu, P., Hu, Y., and Zhang, Y.: FTIR-ATR in situ observation on the efflorescence and deliquescence processes of Mg(NO3)2 aerosols, Sci. China-Chem., 51, 128-137, 2008b.
Li, Y. J., Liu, P. F., Bergoend, C., Bateman, A. P., and Martin, S. T.: Rebounding hygroscopic inorganic aerosol particles: Liquids, gels, and hydrates, Aerosol Sci. Technol., 51, 388-396, 2017.
Liu, Y., Gibson, E. R., Cain, J. P., Wang, H., Grassian, V. H., and Laskin, A.: Kinetics of heterogeneous reaction of $CaCO_3$ particles with gaseous HNO_3 over a wide range of humidity, J. Phys. Chem. A, 112, 1561-1571, 2008a.
Liu, Y. J., Zhu, T., Zhao, D. F., and Zhang, Z. F.: Investigation of the hygroscopic properties of $Ca(NO_3)_2$ and internally mixed $Ca(NO_3)_2/CaCO_3$ particles by micro-Raman spectrometry, Atmos. Chem. Phys., 8, 7205-7215, 2008b.
Ma, Q. X., Liu, Y. C., Liu, C., and He, H.: Heterogeneous Reaction of Acetic Acid on MgO, α-Al_2O_3, and $CaCO_3$ and the Effect on the Hygroscopic Behavior of These Particles, Phys. Chem. Chem. Phys., 14, 8403-8409, 2012.
Mahowald, N., Ward, D. S., Kloster, S., Flanner, M. G., Heald, C. L., Heavens, N. G., Hess, P. G., Lamarque, J.-F., and Chuang, P. Y.: Aerosol Impacts on Climate and Biogeochemistry, Annu. Rev. Environ. Resour., 36, 45-74, 2011.
Mahowald, N. M., Engelstaedter, S., Luo, C., Sealy, A., Artaxo, P., Benitez-Nelson, C., Bonnet, S., Chen, Y., Chuang, P. Y., Cohen, D. D., Dulac, F., Herut, B., Johansen, A. M., Kubilay, N., Losno, R., Maenhaut, W., Paytan, A., Prospero, J. M., Shank, L. M., and Siefert, R. L.: Atmospheric Iron Deposition: Global Distribution, Variability, and Human Perturbations, Ann. Rev. Mar. Sci., 1, 245-278, 2009.
Massoli, P., Lambe, A. T., Ahern, A. T., Williams, L. R., Ehn, M., Mikkila, J., Canagaratna, M. R., Brune, W. H., Onasch, T. B., Jayne, J. T., Petaja, T., Kulmala, M., Laaksonen, A., Kolb, C. E., Davidovits, P., and Worsnop, D. R.: Relationship between aerosol oxidation level and hygroscopic properties of laboratory generated secondary organic aerosol (SOA) particles, Geophys. Res. Lett., 37, L24801, DOI: 24810.21029/22010GL045258, 2010.

Nickovic, S., Vukovic, A., Vujadinovic, M., Djurdjevic, V., and Pejanovic, G.: Technical Note: High-resolution mineralogical database of dust-productive soils for atmospheric dust modeling, Atmos. Chem. Phys., 12, 845-855, 2012.
Pan, X., Uno, I., Hara, Y., Kuribayashi, M., Kobayashi, H., Sugimoto, N., Yamamoto, S., Shimohara, T., and Wang, Z.: Observation of the simultaneous transport of Asian mineral dust aerosols with anthropogenic pollutants using a POPC during a long-lasting dust event in late spring 2014, Geophys. Res. Lett., 42, 1593-1598, 2015.
Pan, X., Uno, I., Wang, Z., Nishizawa, T., Sugimoto, N., Yamamoto, S., Kobayashi, H., Sun, Y., Fu, P., Tang, X., and Wang, Z.: Real-time observational evidence of changing Asian dust morphology with the mixing of heavy anthropogenic pollution, Sci. Rep., 7, 335, doi: 310.1038/s41598-41017-00444-w, 2017.
Pan, X., Ge, B., Wang, Z., Tian, Y., Liu, H., Wei, L., Yue, S., Uno, I., Kobayashi, H., Nishizawa, T., Shimizu, A., Fu, P., and Wang, Z.: Synergistic effect of water-soluble species and relative humidity on morphological changes of aerosol particles in Beijing mega-city during severe pollution episodes, Atmos. Chem. Phys. Discuss., 2018, 1-24, 10.5194/acp-2018-623, 2018.
Pang, S. F., Wu, C. Q., Zhang, Q. N., and Zhang, Y. H.: The structural evolution of magnesium acetate complex in aerosols by FTIR-ATR spectra, J. Mol. Struct., 1087, 46-50, 2015.
Park, K., Kim, J. S., and Miller, A. L.: A study on effects of size and structure on hygroscopicity of nanoparticles using a tandem differential mobility analyzer and TEM, J. Nanopart. Res., 11, 175-183, 2009.
Peng, C., Jing, B., Guo, Y. C., Zhang, Y. H., and Ge, M. F.: Hygroscopic Behavior of Multicomponent Aerosols Involving NaCl and Dicarboxylic Acids, J. Phys. Chem. A, 120, 1029-1038, 2016.
Petters, M. D., and Kreidenweis, S. M.: A single parameter representation of hygroscopic growth and cloud condensation nucleus activity, Atmos. Chem. Phys., 7, 1961-1971, 2007.
Petters, M. D., and Kreidenweis, S. M.: A single parameter representation of hygroscopic growth and cloud condensation nucleus activity-Part 2: Including solubility, Atmos. Chem. Phys., 8, 6273-6279, 2008.
Petters, M. D., Wex, H., Carrico, C. M., Hallbauer, E., Massling, A., McMeeking, G. R., Poulain, L., Wu, Z., Kreidenweis, S. M., and Stratmann, F.: Towards closing the gap between hygroscopic growth and activation for secondary organic aerosol - Part 2: Theoretical approaches, Atmos. Chem. Phys., 9, 3999-4009, 2009.
Prenni, A. J., Petters, M. D., Kreidenweis, S. M., DeMott, P. J., and Ziemann, P. J.: Cloud droplet activation of secondary organic aerosol, J. Geophys. Res.-Atmos., 112, D10223, DOI: 10210.11029/12006JD007963, 2007.
Prince, A. P., Kleiber, P. D., Grassian, V. H., and Young, M. A.: Reactive Uptake of Acetic Acid on Calcite and Nitric Acid Reacted Calcite Aerosol in an Environmental Reaction Chamber, Phys. Chem. Chem. Phys., 10, 142-152, 2008.
Prospero, J. M., Ginoux, P., Torres, O., Nicholson, S. E., and Gill, T. E.: Environmental characterization of global sources of atmospheric soil dust identified with the Nimbus 7 Total Ozone Mapping Spectrometer (TOMS) absorbing aerosol product, Rev. Geophys., 40, 1002, DOI: 1010.1029/2000RG000095, 2002.
Rard, J. A., Habenschuss, A., and Spedding, F. H.: A review of the osmotic coefficients of aqueous calcium chloride at 25 ^{o}C, J. Chem. Eng. Dara, 22, 180-186, 1977.
Rard, J. A., and Miller, D. G.: Isopiestic determination of the osmotic and activity coefficients of aqueous magnesium chloride solutions at 25 ^{o}C, J. Chem. Eng. Dara, 26, 38-43, 1981.
Rard, J. A., Wijesinghe, A. M., and Wolery, T. J.: Review of the thermodynamic properties of Mg(NO3)2(aq) and their representation with the standard and extended ion-interaction (Pitzer) models at 298.15 K, J. Chem. Eng. Data, 49, 1127-1140, 2004.
Ridley, D. A., Heald, C. L., Kok, J. F., and Zhao, C.: An observationally constrained estimate of global dust aerosol optical depth, Atmos. Chem. Phys., 16, 15097-15117, 2016.
Robinson, R. A., and Stokes, R. H.: Electrolyte Solutions (Second Revised Edition), Butterworths, London, UK, 1959.
Romanias, M. N., El Zein, A., and Bedjanian, Y.: Heterogeneous Interaction of H_2O_2 with TiO_2 Surface under Dark and UV Light Irradiation Conditions, J. Phys. Chem. A, 116, 8191-8200, 2012.
Romanias, M. N., Zeineddine, M. N., Gaudion, V., Lun, X., Thevenet, F., and Riffault, V.: Heterogeneous Interaction of Isopropanol with Natural Gobi Dust, Environ. Sci. Technol., 50, 11714-11722, 2016.
Santschi, C., and Rossi, M. J.: Uptake of CO_2, SO_2, HNO_3 and HCl on calcite ($CaCO_3$) at 300 K: Mechanism and the role of adsorbed water, J. Phys. Chem. A, 110, 6789-6802, 2006.
Scanza, R. A., Mahowald, N., Ghan, S., Zender, C. S., Kok, J. F., Liu, X., Zhang, Y., and Albani, S.: Modeling Dust as Component Minerals in the Community Atmosphere Model: Development of Framework and Impact on Radiative Forcing, Atmos. Chem. Phys., 15, 537-561, 2015.
Seinfeld, J. H., and Pandis, S. N.: Atmospheric Chemistry and Physics: From Air Pollution to Climate Change, Wiley Interscience, New York, 2006.

Shi, Z., Zhang, D., Hayashi, M., Ogata, H., Ji, H., and Fujiie, W.: Influences of sulfate and nitrate on the hygroscopic behaviour of coarse dust particles, Atmos. Environ., 42, 822-827, 2008.
Sullivan, R. C., Moore, M. J. K., Petters, M. D., Kreidenweis, S. M., Roberts, G. C., and Prather, K. A.: Effect of Chemical Mixing State on the Hygroscopicity and Cloud Nucleation Properties of Calcium Mineral Dust Particles, Atmos. Chem. Phys., 9, 3303-3316, 2009.
Tan, F., Tong, S. R., Jing, B., Hou, S., Liu, Q., Li, K., Zhang, Y., and Ge, M. F.: Heterogeneous reactions of NO2 with $CaCO_3$–$(NH_4)_2SO_4$ mixtures at different relative humidities, Atmos. Chem. Phys., 16, 8081-8093, 2016.
Tang, I. N., and Fung, K. H.: Hydration and Raman scattering studies of levitated microparticles: $Ba(NO_3)_2$, $Sr(NO_3)_2$, and $Ca(NO_3)_2$, J. Chem. Phys., 106, 1653-1660, 1997.
Tang, M. J., Thieser, J., Schuster, G., and Crowley, J. N.: Kinetics and Mechanism of the Heterogeneous Reaction of N_2O_5 with Mineral Dust Particles, Phys. Chem. Chem. Phys., 14, 8551-8561, 2012.
Tang, M. J., Whitehead, J., Davidson, N. M., Pope, F. D., Alfarra, M. R., McFiggans, G., and Kalberer, M.: Cloud Condensation Nucleation Activities of Calcium Carbonate and its Atmospheric Ageing Products, Phys. Chem. Chem. Phys., 17, 32194-32203, 2015.
Tang, M. J., Cziczo, D. J., and Grassian, V. H.: Interactions of Water with Mineral Dust Aerosol: Water Adsorption, Hygroscopicity, Cloud Condensation and Ice Nucleation, Chem. Rev., 116, 4205–4259, 2016a.
Tang, M. J., Larish, W., Fang, Y., Gankanda, A., and Grassian, V. H.: Heterogeneous Reactions of Acetic Acid with Oxide Surfaces: Effects of Mineralogy and Relative Humidity, J. Phys. Chem. A, 120, 5609-5616, 2016b.
Tang, M. J., Huang, X., Lu, K. D., Ge, M. F., Li, Y. J., Cheng, P., Zhu, T., Ding, A. J., Zhang, Y. H., Gligorovski, S., Song, W., Ding, X., Bi, X. H., and Wang, X. M.: Heterogeneous reactions of mineral dust aerosol: implications for tropospheric oxidation capacity, Atmos. Chem. Phys., 17, 11727-11777, 2017.
Textor, C., Schulz, M., Guibert, S., Kinne, S., Balkanski, Y., Bauer, S., Berntsen, T., Berglen, T., Boucher, O., Chin, M., Dentener, F., Diehl, T., Easter, R., Feichter, H., Fillmore, D., Ghan, S., Ginoux, P., Gong, S., Grini, A., Hendricks, J., Horowitz, L., Huang, P., Isaksen, I., Iversen, I., Kloster, S., Koch, D., Kirkevåg, A., Kristjansson, J. E., Krol, M., Lauer, A., Lamarque, J. F., Liu, X., Montanaro, V., Myhre, G., Penner, J., Pitari, G., Reddy, S., Seland, Ø., Stier, P., Takemura, T., and Tie, X.: Analysis and Quantification of the Diversities of Aerosol Life Cycles within AeroCom, Atmos. Chem. Phys., 6, 1777-1813, 2006.
Tobo, Y., Zhang, D. Z., Nakata, N., Yamada, M., Ogata, H., Hara, K., and Iwasaka, Y.: Hygroscopic mineral dust particles as influenced by chlorine chemistry in the marine atmosphere, Geophys. Res. Lett., 36, L05817, doi: 05810.01029/02008gl036883, 2009.
Tobo, Y., Zhang, D., Matsuki, A., and Iwasaka, Y.: Asian Dust Particles Converted into Aqueous Droplets under Remote Marine Atmospheric Conditions, Proc. Natl. Acad. Sci. U. S. A., 107, 17905-17910, 2010.
Tong, S. R., Wu, L. Y., Ge, M. F., Wang, W. G., and Pu, Z. F.: Heterogeneous Chemistry of Monocarboxylic Acids on α-Al_2O_3 at Different Relative Humidities, Atmos. Chem. Phys., 10, 7561-7574, 2010.
Uno, I., Eguchi, K., Yumimoto, K., Takemura, T., Shimizu, A., Uematsu, M., Liu, Z., Wang, Z., Hara, Y., and Sugimoto, N.: Asian Dust Transported One Full Circuit around the Globe, Nature Geosci., 2, 557-560, 2009.
Usher, C. R., Michel, A. E., and Grassian, V. H.: Reactions on Mineral Dust, Chem. Rev., 103, 4883-4939, 2003.
Vlasenko, A., Sjogren, S., Weingartner, E., Stemmler, K., Gaggeler, H. W., and Ammann, M.: Effect of Humidity on Nitric Acid Uptake to Mineral Dust Aerosol Particles, Atmos. Chem. Phys., 6, 2147-2160, 2006.
Vlasenko, S. S., Su, H., Pöschl, U., Andreae, M. O., and Mikhailov, E. F.: Tandem configuration of differential mobility and centrifugal particle mass analysers for investigating aerosol hygroscopic properties, Atmos. Meas. Tech., 10, 1269-1280, 2017.
Wang, L. Y., Zhang, Y. H., and Zhao, L. J.: Raman spectroscopic studies on single supersaturated droplets of sodium and magnesium acetate, J. Phys. Chem. A, 109, 609-614, 2005.
Wex, H., Petters, M. D., Carrico, C. M., Hallbauer, E., Massling, A., McMeeking, G. R., Poulain, L., Wu, Z., Kreidenweis, S. M., and Stratmann, F.: Towards closing the gap between hygroscopic growth and activation for secondary organic aerosol: Part 1 – Evidence from measurements, Atmos. Chem. Phys., 9, 3987-3997, 2009.
Wexler, A. S., and Seinfeld, J. H.: 2nd generation inorganic aerosol model, Atmos. Environ., 25, 2731-2748, 1991.
Zhang, Y., Mahowald, N., Scanza, R. A., Journet, E., Desboeufs, K., Albani, S., Kok, J. F., Zhuang, G., Chen, Y., Cohen, D. D., Paytan, A., Patey, M. D., Achterberg, E. P., Engelbrecht, J. P., and Fomba, K. W.: Modeling the global emission, transport and deposition of trace elements associated with mineral dust, Biogeosciences, 12, 5771-5792, 2015.
Zhang, Y. H., Choi, M. Y., and Chan, C. K.: Relating hygroscopic properties of magnesium nitrate to the formation of contact ion pairs, J. Phys. Chem. A, 108, 1712-1718, 2004.

1011 Zieger, P., Vaisanen, O., Corbin, J. C., Partridge, D. G., Bastelberger, S., Mousavi-Fard, M., Rosati, B., Gysel, M.,
1012 Krieger, U. K., Leck, C., Nenes, A., Riipinen, I., Virtanen, A., and Salter, M. E.: Revising the hygroscopicity of
1013 inorganic sea salt particles, Nature Communications, 8, 15883, doi: 15810.11038/ncomms15883, 2017.
1014